

K. H.-L. Chau, et. al.. "Pressure and Sound Measurement."

Copyright 2000 CRC Press LLC. <<http://www.engnetbase.com>>.

Pressure and Sound Measurement

Kevin H.-L. Chau

Analog Devices, Inc.

Ron Goehner

The Fredericks Company

Emil Drubetsky

The Fredericks Company

Howard M. Brady

The Fredericks Company

William H. Bayles, Jr.

The Fredericks Company

Peder C. Pedersen

Worcester Polytechnic Institute

- 26.1 Pressure Measurement
Basic Definitions • Sensing Principles • Silicon
Micromachined Pressure Sensors
- 26.2 Vacuum Measurement
Background and History of Vacuum Gages • Direct Reading
Gages • Indirect Reading Gages
- 26.3 Ultrasound Measurement
Applications of Ultrasound • Definition of Basic Ultrasound
Parameters • Conceptual Description of Ultrasound Imaging
and Measurements • Single-Element and Array Transducers •
Selection Criteria for Ultrasound Frequencies • Basic
Parameters in Ultrasound Measurements • Ultrasound
Theory and Applications • Review of Common Applications
of Ultrasound and Their Instrumentation • Selected
Manufacturers of Ultrasound Products • Advanced Topics
in Ultrasound

26.1 Pressure Measurement

Kevin H.-L. Chau

Basic Definitions

Pressure is defined as the normal force per unit area exerted by a fluid (liquid or gas) on any surface. The surface can be either a solid boundary in contact with the fluid or, for purposes of analysis, an imaginary plane drawn through the fluid. Only the component of the force normal to the surface needs to be considered for the determination of pressure. Tangential forces that give rise to shear and fluid motion will not be a relevant subject of discussion here. In the limit that the surface area approaches zero, the ratio of the differential normal force to the differential area represents the pressure at a point on the surface. Furthermore, if there is no shear in the fluid, the pressure at any point can be shown to be independent of the orientation of the imaginary surface under consideration. Finally, it should be noted that pressure is not defined as a vector quantity and is therefore nondirectional.

Three types of pressure measurements are commonly performed:

Absolute pressure is the same as the pressure defined above. It represents the pressure difference between the point of measurement and a perfect vacuum where pressure is zero.

Gage pressure is the pressure difference between the point of measurement and the ambient. In reality, the ambient (atmospheric) pressure can vary, but only the pressure difference is of interest in gage pressure measurements.

TABLE 26.1 Pressure Unit Conversion Table

Units	kPa	psi	in H ₂ O	cm H ₂ O	in. Hg	mm Hg	mbar
kPa	1.000	0.1450	4.015	10.20	0.2593	7.501	10.00
psi	6.895	1.000	27.68	70.31	2.036	51.72	68.95
in. H ₂ O	0.2491	3.613×10^{-2}	1.000	2.540	7.355×10^{-2}	1.868	2.491
cm H ₂ O	0.09806	1.422×10^{-2}	0.3937	1.000	2.896×10^{-2}	0.7355	0.9806
in. Hg	3.386	0.4912	13.60	34.53	1.000	25.40	33.86
mm Hg	0.1333	1.934×10^{-2}	0.5353	1.360	3.937×10^{-2}	1.000	1.333
mbar	0.1000	0.01450	0.04015	1.020	0.02953	0.7501	1.000

Key:

- (1) kPa = kilopascal;
- (2) psi = pound force per square inch;
- (3) in. H₂O = inch of water at 4°C;
- (4) cm H₂O = centimeter of water at 4°C;
- (5) in. Hg = inch of mercury at 0°C;
- (6) mm Hg = millimeter of mercury at 0°C;
- (7) mbar = millibar.

Differential pressure is the pressure difference between two points, one of which is chosen to be the reference. In reality, both pressures can vary, but only the pressure difference is of interest here.

Units of Pressure and Conversion

The SI unit of pressure is the *pascal* (Pa), which is defined as the newton per square meter ($\text{N}\cdot\text{m}^{-2}$); 1 Pa is a very small unit of pressure. Hence, decimal multiples of the pascal (e.g., kilopascals [kPa] and megapascals [MPa]) are often used for expressing higher pressures. In weather reports, the hectopascal (1 hPa = 100 Pa) has been adopted by many countries to replace the millibar (1 bar = 10^5 Pa; hence, 1 millibar = 10^{-3} bar = 1 hPa) as the unit for atmospheric pressure. In the United States, pressure is commonly expressed in pound force per square inch (psi), which is about 6.90 kPa. In addition, the absolute, gage, and differential pressures are further specified as psia, psig, and psid, respectively. However, no such distinction is made in any pressure units other than the psi. There is another class of units e.g., millimeter of mercury at 0°C (mm Hg, also known as the *torr*) or inch of water at 4°C (in H₂O), which expresses pressure in terms of the height of a static liquid column. The actual pressure p referred to is one that will be developed at the base of the liquid column due to its weight, which is given by Equation 26.1.

$$p = \rho g h \quad (26.1)$$

where ρ is the density of the liquid, g is the acceleration due to gravity, and h is the height of the liquid column. A conversion table for the most popular pressure units is provided in [Table 26.1](#).

Sensing Principles

Sensing Elements

Since pressure is defined as the force per unit area, the most direct way of measuring pressure is to isolate an area on an elastic mechanical element for the force to act on. The deformation of the sensing element produces displacements and strains that can be precisely sensed to give a calibrated measurement of the pressure. This forms the basis for essentially all commercially available pressure sensors today. Specifically, the basic requirements for a pressure-sensing element are a means to isolate two fluidic pressures (one to be measured and the other one as the reference) and an elastic portion to convert the pressure difference into a deformation of the sensing element. Many types of pressure-sensing elements are currently in use. These can be grouped as diaphragms, capsules, bellows, and tubes, as illustrated in [Figure 26.1](#). Diaphragms

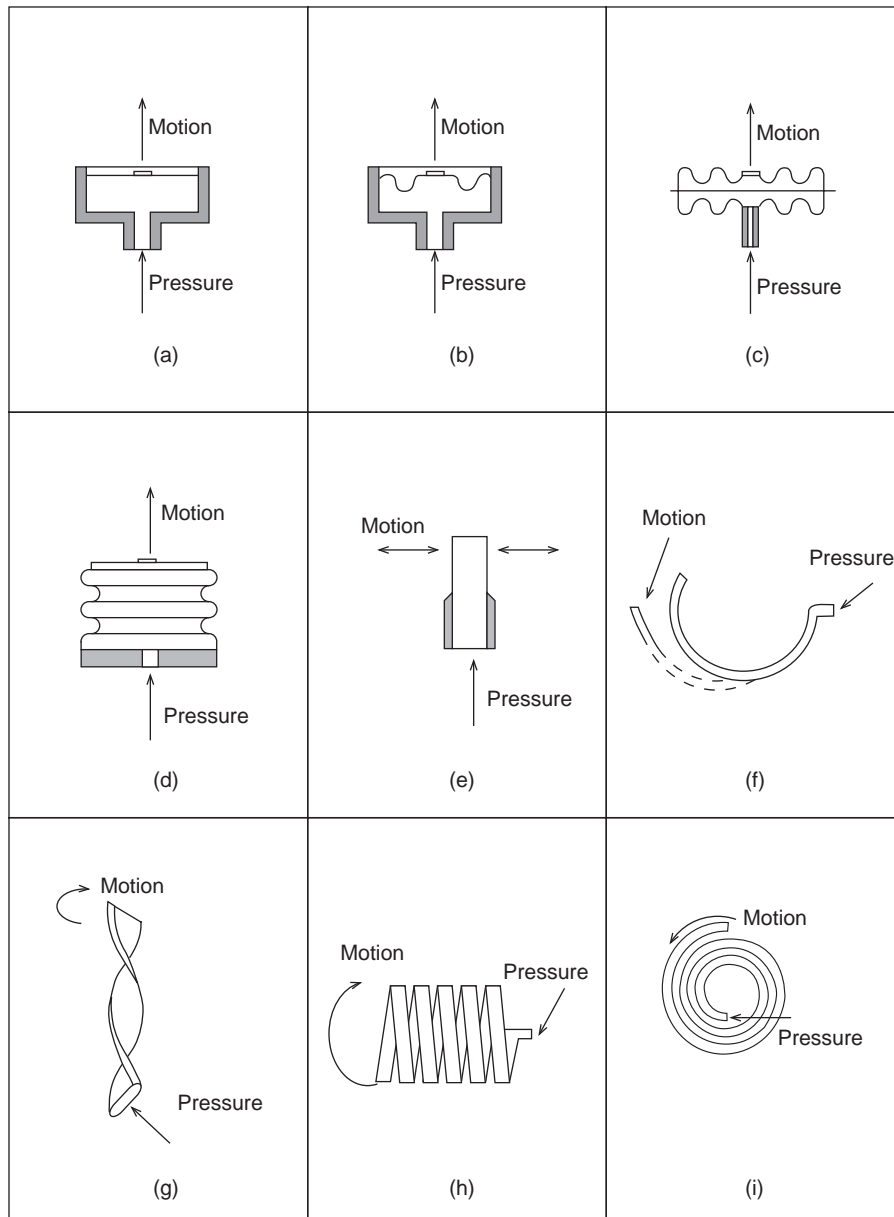


FIGURE 26.1 Pressure-sensing elements: (a) flat diaphragm; (b) corrugated diaphragm; (c) capsule; (d) bellows; (e) straight tube; (f) C-shaped Bourdon tube; (g) twisted Bourdon tube; (h) helical Bourdon tube; (i) spiral Bourdon tube.

are by far the most widely used of all sensing elements. A special form of tube, known as the *Bourdon tube*, is curved or twisted along its length and has an oval cross-section. The tube is sealed at one end and tends to unwind or straighten when it is subjected to a pressure applied to the inside. In general, Bourdon tubes are designed for measuring high pressures, while capsules and bellows are usually for measuring low pressures. A detailed description of these sensing elements can be found in [1].

Detection Methods

A detection means is required to convert the deformation of the sensing element into a pressure readout. In the simplest approach, the displacements of a sensing element can be amplified mechanically by lever and flexure linkages to drive a pointer over a graduated scale, for example, in the moving pointer barometers. Some of the earliest pressure sensors employed a Bourdon tube to drive the wiper arm over a potentiometric resistance element. In *linear-variable differential-transformer* (LVDT) pressure sensors, the displacement of a Bourdon tube or capsule is used to move a magnetic core inside a coil assembly to vary its inductance. In *piezoelectric* pressure sensors, the strains associated with the deformation of a sensing element are converted into an electrical charge output by a piezoelectric crystal. Piezoelectric pressure sensors are useful for measuring high-pressure transient events, for example, explosive pressures. In *vibrating-wire* pressure sensors, a metal wire (typically tungsten) is stretched between a fixed anchor and the center of a diaphragm. The wire is located near a permanent magnet and is set into vibration at its resonant frequency by an ac current excitation. A pressure-induced displacement of the diaphragm changes the tension and therefore the resonant frequency of the wire, which is measured by the readout electronics. A detailed description of these and other types of detection methods can be found in [1].

Capacitive Pressure Sensors.

Many highly accurate (better than 0.1%) pressure sensors in use today have been developed using the capacitive detection approach. Capacitive pressure sensors can be designed to cover an extremely wide pressure range. Both high-pressure sensors with full-scale pressures above 10^7 Pa (a few thousand psi) and vacuum sensors (commonly referred to as capacitive *manometers*) usable for pressure measurements below 10^{-3} Pa (10^{-5} torr) are commercially available. The principle of *capacitive pressure sensors* is illustrated in [Figure 26.2](#). A metal or silicon diaphragm serves as the pressure-sensing element and constitutes one electrode of a capacitor. The other electrode, which is stationary, is typically formed by a deposited metal layer on a ceramic or glass substrate. An applied pressure deflects the diaphragm, which in turn changes the gap spacing and the capacitance [2]. In the differential capacitor design, the sensing diaphragm is located in between two stationary electrodes. An applied pressure will cause one capacitance to increase and the other one to decrease, thus resulting in twice the signal while canceling many undesirable common mode effects. [Figure 26.3](#) shows a practical design of a differential capacitive sensing cell that uses two isolating diaphragms and an oil fill to transmit the differential pressure to the sensing diaphragm. The isolating diaphragms are made of special metal alloys that enable them to handle corrosive fluids. The oil is chosen to set a predictable dielectric constant for the capacitor gaps while providing adequate damping to reduce shock and vibration effects. [Figure 26.4](#) shows a rugged capacitive pressure sensor for industrial applications based on the capacitive sensing cell shown in [Figure 26.3](#). The capacitor electrodes are connected to the readout electronics housing at the top. In general, with today's sophisticated electronics and special considerations to minimize stray capacitances (that can degrade the accuracy of measurements), a capacitance change of 10 aF (10^{-18} F) provided by a diaphragm deflection of only a fraction of a nanometer is resolvable.

Piezoresistive Pressure Sensors.

Piezoresistive sensors (also known as *strain-gage* sensors) are the most common type of pressure sensor in use today. *Piezoresistive effect* refers to a change in the electric resistance of a material when stresses or strains are applied. Piezoresistive materials can be used to realize strain gages that, when incorporated into diaphragms, are well suited for sensing the induced strains as the diaphragm is deflected by an applied pressure. The sensitivity of a strain gage is expressed by its *gage factor*, which is defined as the fractional change in resistance, $\Delta R/R$, per unit strain:

$$\text{Gage factor} = \left(\frac{\Delta R}{R} \right) / \epsilon \quad (26.2)$$

where strain ϵ is defined as $\Delta L/L$, or the extension per unit length. It is essential to distinguish between two different cases in which: (1) the strain is parallel to the direction of the current flow (along which

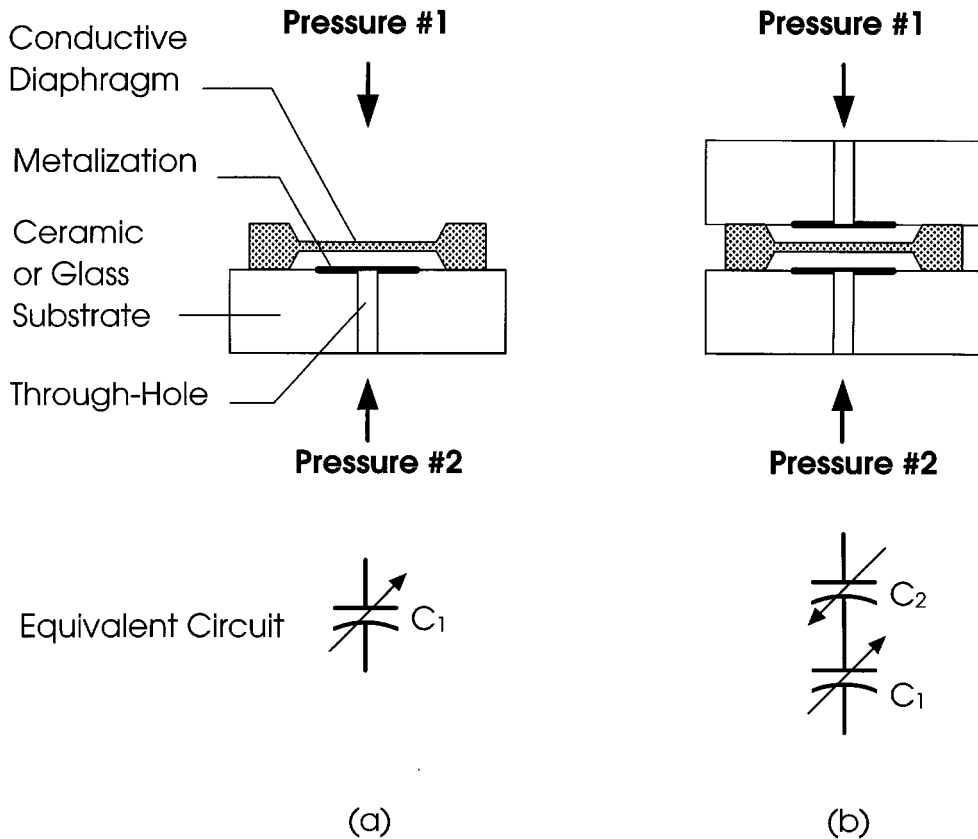


FIGURE 26.2 Operating principle of capacitive pressure sensors. (a) Single capacitor design; and (b) differential capacitor design.

the resistance change is to be monitored); and (2) the strain is perpendicular to the direction of the current flow. The gage factors associated with these two cases are known as the *longitudinal gage factor* and the *transverse gage factor*, respectively. The two gage factors are generally different in magnitude and often opposite in sign. Typical longitudinal gage factors are ~ 2 for many useful metals, 10 to 35 for polycrystalline silicon (polysilicon), and 50 to 150 for single-crystalline silicon [3–5]. Because of its large piezoresistive effect, silicon has become the most commonly used material for strain gages. There are several ways to incorporate strain gages into pressure-sensing diaphragms. For example, strain gages can be directly bonded onto a metal diaphragm. However, hysteresis and creep of the bonding agent are potential issues. Alternatively, the strain gage material can be deposited as a thin film on the diaphragm. The adhesion results from strong molecular forces that will not creep, and no additional bonding agent is required. Today, the majority of piezoresistive pressure sensors are realized by integrating the strain gages into the silicon diaphragm using integrated circuit fabrication technology. This important class of silicon pressure sensors will be discussed in detail in the next section.

Silicon Micromachined Pressure Sensors

Silicon micromachined pressure sensors refer to a class of pressure sensors that employ integrated circuit batch processing techniques to realize a thinned-out diaphragm sensing element on a silicon chip. Strain gages made of silicon diffused resistors are typically integrated on the diaphragm to convert the pressure-induced diaphragm deflection into an electric resistance change. Over the past 20 years, silicon micro-machined pressure sensors have gradually replaced their mechanical counterparts and have captured over

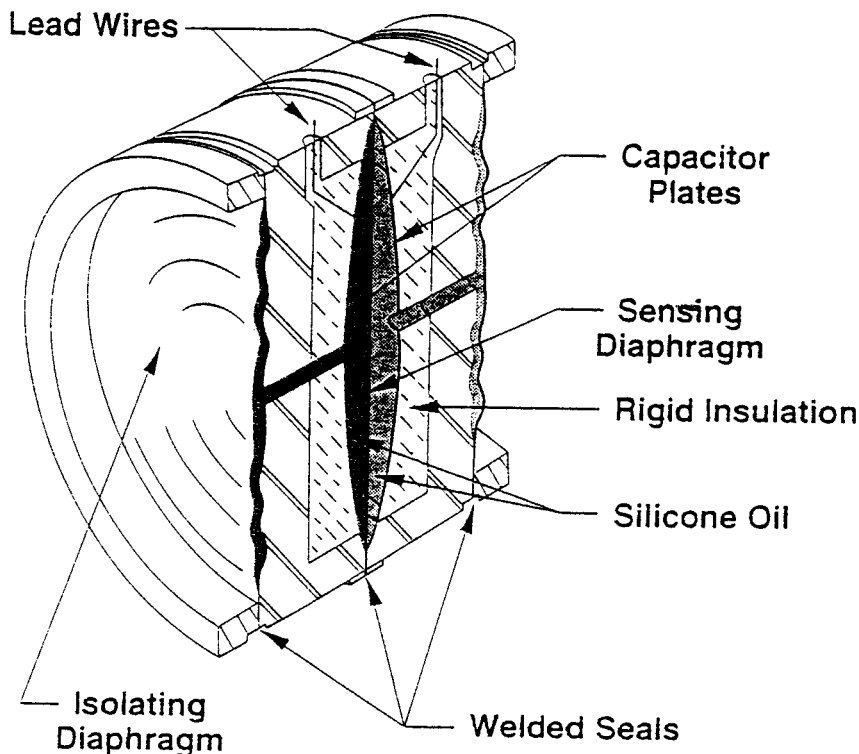


FIGURE 26.3 A differential capacitive sensing cell that is equipped with isolating diaphragms and silicone oil transfer fluid suitable for measuring pressure in corrosive media. (Courtesy of Rosemount, Inc.)

80% of the pressure sensor market. There are several unique advantages that silicon offers. Silicon is an ideal mechanical material that does not display any hysteresis or yield and is elastic up to the fracture limit. It is stronger than steel in yield strength and comparable in Young's modulus [6]. As mentioned in the previous section, the piezoresistive effect in single-crystalline silicon is almost 2 orders of magnitude larger than that of metal strain gages. Silicon has been widely used in integrated circuit manufacturing for which reliable batch fabrication technology and high-precision dimension control techniques have been well developed. A typical silicon wafer yields hundreds of identical pressure sensor chips at very low cost. Further, the necessary signal conditioning circuitry can be integrated on the same sensor chip no more than a few millimeters in size [7]. All these are key factors that contributed to the success of silicon micromachined pressure sensors.

Figure 26.5 shows a typical construction of a silicon piezoresistive pressure sensor. An array of square or rectangular diaphragms is "micromachined" out of a (100) oriented single-crystalline silicon wafer by selectively removing material from the back. An anisotropic silicon etchant (e.g., potassium hydroxide) is typically employed; it etches fastest on (100) surfaces and much slower on (111) surfaces. The result is a pit formed on the backside of the wafer bounded by (111) surfaces and a thinned-out diaphragm section on the front at every sensor site. The diaphragm thickness is controlled by a timed etch or by using suitable etch-stop techniques [6, 8]. To realize strain gages, *p*-type dopant, typically boron, is diffused into the front of the *n*-type silicon diaphragm at stress-sensitive locations to form resistors that are electrically isolated from the diaphragm and from each other by reverse biased *p-n* junctions. The strain gages, the diaphragm, and the rest of the supporting sensor chip all belong to the same single-crystalline silicon. The result is a superb mechanical structure that is free from creep, hysteresis, and thermal expansion coefficient mismatches. However, the sensor die must still be mounted to a sensor housing, which typically has mechanical properties different from that of silicon. It is crucial to ensure



FIGURE 26.4 A rugged capacitive pressure sensor product for industrial applications. It incorporates the sensing cell shown in Figure 26.3. Readout electronics are contained in the housing at the top. (Courtesy of Rosemount, Inc.)

a high degree of stress isolation between the sensor housing and the sensing diaphragm that may otherwise lead to long-term mechanical drifts and undesirable temperature behavior. A common practice is to bond a glass wafer or a second silicon wafer to the back of the sensor wafer to reinforce the overall composite sensor die. This way, the interface stresses generated by the die mount will also be sufficiently remote from the sensing diaphragm and will not seriously affect its stress characteristics. For gage or differential pressure sensing, holes must be provided through the carrier wafer prior to bonding that are aligned to the etch pits of the sensor wafer leading to the back of the sensing diaphragms. No through holes are necessary for absolute pressure sensing. The wafer-to-wafer bonding is performed in a vacuum to achieve a sealed reference vacuum inside the etch pit [6, 9]. Today's silicon pressure sensors are available in a large variety of plastic, ceramic, metal can, and stainless steel packages (some examples are shown in Figure 26.6). Many are suited for printed circuit board mounting. Others have isolating diaphragms and transfer fluids for handling corrosive media. They can be readily designed for a wide range of industrial, medical, automotive, aerospace, and military applications.

Silicon Piezoresistive Pressure Sensor Limitations

Despite the relatively large piezoresistive effects in silicon strain gages, the full-scale resistance change is typically only 1% to 2% of the resistance of the strain gage (which yields an unamplified voltage output of 10 mV/V to 20 mV/V). To achieve an overall accuracy of 0.1% of full scale, for example, the combined effects of mechanical and electrical repeatability, hysteresis, linearity, and stability must be controlled or compensated to within a few parts per million (ppm) of the gage resistance. Furthermore, silicon strain gages are also very temperature sensitive and require careful compensations. There are two primary sources of temperature drifts: (1) the temperature coefficient of resistance of the strain gages (from 0.06%/°C to 0.24%/°C); and (2) the temperature coefficient of the gage factors (from -0.06%/°C to

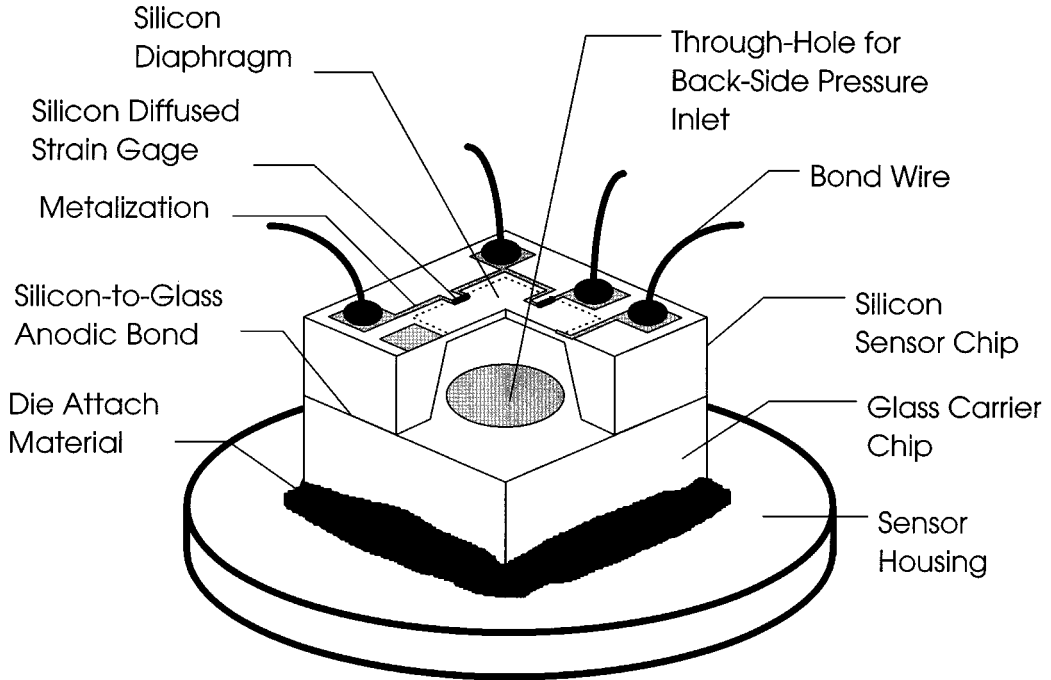


FIGURE 26.5 A cut-away view showing the typical construction of a silicon piezoresistive pressure sensor.



FIGURE 26.6 Examples of commercially available packages for silicon pressure sensors. Shown in the photo are surface-mount units, dual-in-line (DIP) units, TO-8 metal cans, and stainless steel units with isolating diaphragms. (Courtesy of EG&G IC Sensors.)

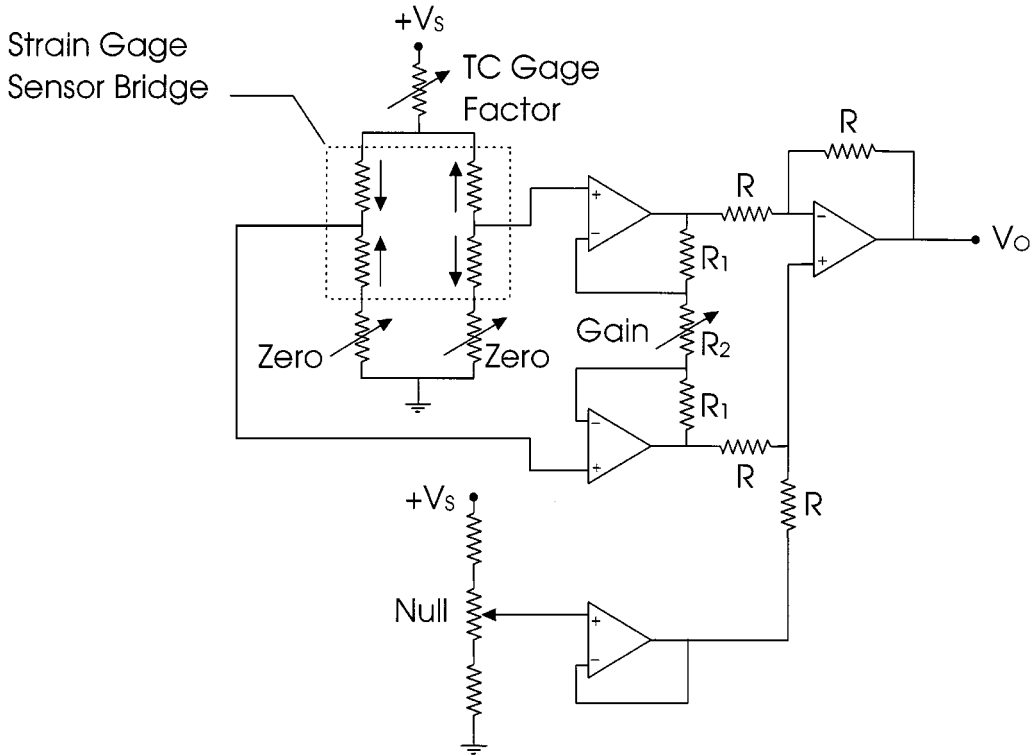


FIGURE 26.7 A signal-conditioning circuit for silicon piezoresistive pressure sensor.

−0.24%/°C), which will cause a decrease in pressure sensitivity as the temperature rises. Figure 26.7 shows a circuit configuration that can be used to achieve offset (resulting from gage resistance mismatch) and temperature compensations as well as providing signal amplification to give a high-level output. Four strain gages that are closely matched in both their resistances and temperature coefficients of resistance are employed to form the four active arms of a Wheatstone bridge. Their resistor geometry on the sensing diaphragm is aligned with the principal strain directions so that two strain gages will produce a resistance increase and the other two a resistance decrease on a given diaphragm deflection. These two pairs of strain gages are configured in the Wheatstone bridge such that an applied pressure will produce a bridge resistance imbalance while the temperature coefficient of resistance will only cause a common mode resistance change in all four gages, keeping the bridge balanced. As for the temperature coefficient of the gage factor, because it is always negative, it is possible (e.g., with the voltage divider circuit in Figure 26.7) to utilize the positive temperature coefficient of the bridge resistance to increase the bridge supply voltage, compensating for the loss in pressure sensitivity as temperature rises. Another major limitation in silicon pressure sensors is the nonlinearity in the pressure response that usually arises from the slight nonlinear behavior in the diaphragm mechanical and the silicon piezoresistive characteristics. The nonlinearity in the pressure response can be compensated by using analog circuit components. However, for the most accurate silicon pressure sensors, digital compensation using a microprocessor with correction coefficients stored in memory is often employed to compensate for all the predictable temperature and nonlinear characteristics. The best silicon pressure sensors today can achieve an accuracy of 0.08% of full scale and a long-term stability of 0.1% of full scale per year. Typical compensated temperature range is from −40°C to 85°C, with the errors of compensation on span and offset both around 1% of full scale. Commercial products are currently available for full-scale pressure ranges from 10 kPa to 70 MPa (1.5 psi to 10,000 psi). The 1998 prices are U.S.\$5 to \$20 for the most basic uncompensated sensors; \$10 to \$50 for the compensated (with additional laser trimmed resistors either integrated on-chip or on a ceramic substrate)

TABLE 26.2 Selected Companies That Make Pressure Sensors and Pressure Calibration Systems
(This is not intended to be an exhaustive list of all manufacturers.)

(1) Silicon micromachined piezoresistive pressure sensor	(2) Bonded strain gage pressure sensors
Druck Inc. 4 Dunham Drive New Fairfield, CT 06812 Tel: (203) 746-0400 http://www.druck.com	Gefran Inc. 122 Terry Dr. Newtown, PA 18940 Tel: (215) 968-6238 http://www.gefran.it
EG&G IC Sensors 1701 McCarthy Blvd. Milpitas, CA 95035-7416 Tel: (408) 432-1800	(3) Capacitive pressure sensors
Foxboro ICT 199 River Oaks Pkwy. San Jose, CA 95134-1996 Tel: (408) 432-1010	Kavlico Corp. 14501 Los Angeles Ave. Moorpark, CA 93021 Tel: (805) 523-2000
Honeywell Inc. Micro Switch Div. 11 W. Spring St. Freeport, IL 61032-4353 Tel: (815) 235-5500 http://www.honeywell.com/sensing	Rosemount Inc. Measurement Div. 12001 Technology Drive Eden Prairie, MN 55344 Tel: (800) 999-9307 http://www.rosemount.com
Lucas NovaSensor 1055 Mission Ct. Fremont, CA 94539 Tel: (800) 962-7364 http://www.novasensor.com	(4) Pressure calibration systems
Motorola, Inc. Sensor Products Div. 5005 E. McDowell Rd. Phoenix, AZ 85008 Tel: (602) 244-3381 http://mot-sps.com/senseon	Mensor Corp. 2230 IH-35 South San Marcos, TX 78666-5917 Tel: (512) 396-4200 http://www.mensor.com
SenSym, Inc. 1804 McCarthy Blvd. Milpitas, CA 95035 Tel: (408) 954-1100 http://www.sensym.com	Ruska Instrument 10311 Westpark Drive Houston, TX 77042 Tel: (713) 975-0547 http://www.ruska.com

or signal-conditioned (compensated with amplified output) sensors; and \$60 to \$300 for sensors with isolating diaphragms in stainless steel housings. Table 26.2 provides contact information for selected companies making pressure sensors.

References

1. H. N. Norton, *Handbook of Transducers*, Englewood Cliffs, NJ: Prentice-Hall, 1989, 294-330.
2. W. H. Ko, Solid-state capacitive pressure transducers, *Sensors and Actuators*, 10, 303-320, 1986.
3. C. S. Smith, Piezoresistance effect in germanium and silicon, *Phys. Rev.*, 94, 42-49, 1954.
4. O. N. Tufte and E. L. Stelzer, Piezoresistive properties of silicon diffused layers, *J. Appl. Phys.*, 34, 313-318, 1963.

5. D. Schubert, W. Jenschke, T. Uhlig, and F. M. Schmidt, Piezoresistive properties of polycrystalline and crystalline silicon films, *Sensors and Actuators*, 11, 145-155, 1987.
6. K. E. Petersen, Silicon as a mechanical material, *IEEE Proc.*, 70, 420-457, 1982.
7. R. F. Wolffenbittel (ed.), *Silicon Sensors and Circuits: On-Chip Compatibility*, London: Chapman & Hall, 1996, 171-210.
8. H. Seidel, The mechanism of anisotropic silicon etching and its relevance for micromachining, Tech. Dig., *Transducers '87*, Tokyo, Japan, June 1987, 120-125.
9. E. P. Shankland, Piezoresistive silicon pressure sensors, *Sensors*, 22-26, Aug. 1991.

Further Information

- R. S. Muller, R. T. Howe, S. D. Senturia, R. L. Smith, and R. M. White (eds.), *Microsensors*, New York: IEEE Press, 1991, provides an excellent collection of papers on silicon microsensors and silicon micromachining technologies.
- R. F. Wolffenbittel (ed.), *Silicon Sensors and Circuits: On-Chip Compatibility*, London: Chapman & Hall, 1996, provides a thorough discussion on sensor and circuit integration.
- ISA Directory of Instrumentation On-Line (<http://www.isa.org>) from the Instrument Society of America maintains a list of product categories and active links to many sensor manufacturers.

26.2 Vacuum Measurement

*Ron Goehner, Emil Drubetsky, Howard M. Brady,
and William H. Bayles, Jr.*

Background and History of Vacuum Gages

To make measurements in the vacuum region, one must possess a knowledge of the expected pressure range required by the processes taking place in the vacuum chamber as well as the accuracy and/or repeatability of the measurement required for the process. Typical vacuum systems require that many orders of magnitude of pressures must be measured. In many applications, the pressure range may be 8 orders of magnitude, or from atmospheric (1.01×10^5 Pa, 760 torr) to 1×10^{-3} Pa (7.5×10^{-6} torr).

For semiconductor lithography, high-energy physics experiments and surface chemistry, ultimate vacuum of 7.5×10^{-9} torr and much lower are required (a range of 11 orders of magnitude below atmospheric pressure). One gage will not give reasonable measurements over such large pressure ranges. Over the past 50 years, vacuum measuring instruments (commonly called gages) have been developed that used transducers (or sensors) which can be classified as either direct reading (usually mechanical) or indirect reading [1] (usually electronic). Figure 26.8 shows vacuum gages typically in current use. When a force on a surface is used to measure pressure, the gages are mechanical and are called *direct reading* gages, whereas when any property of the gas that changes with density is measured by electronic means, they are called *indirect reading* gages. Figure 26.9 shows the range of operating pressure for various types of vacuum gages.

Direct Reading Gages

A subdivision of direct reading gages can be made by dividing them into those that utilize a liquid wall and those that utilize a solid wall. The force exerted on a surface from the pressure of thermally agitated molecules and atoms is used to measure the pressure.

Liquid Wall Gages

The two common gages that use a liquid wall are the manometer and the McLeod gage. The liquid column *manometer* is the simplest type of vacuum gage. It consists of a straight or U-shaped glass tube

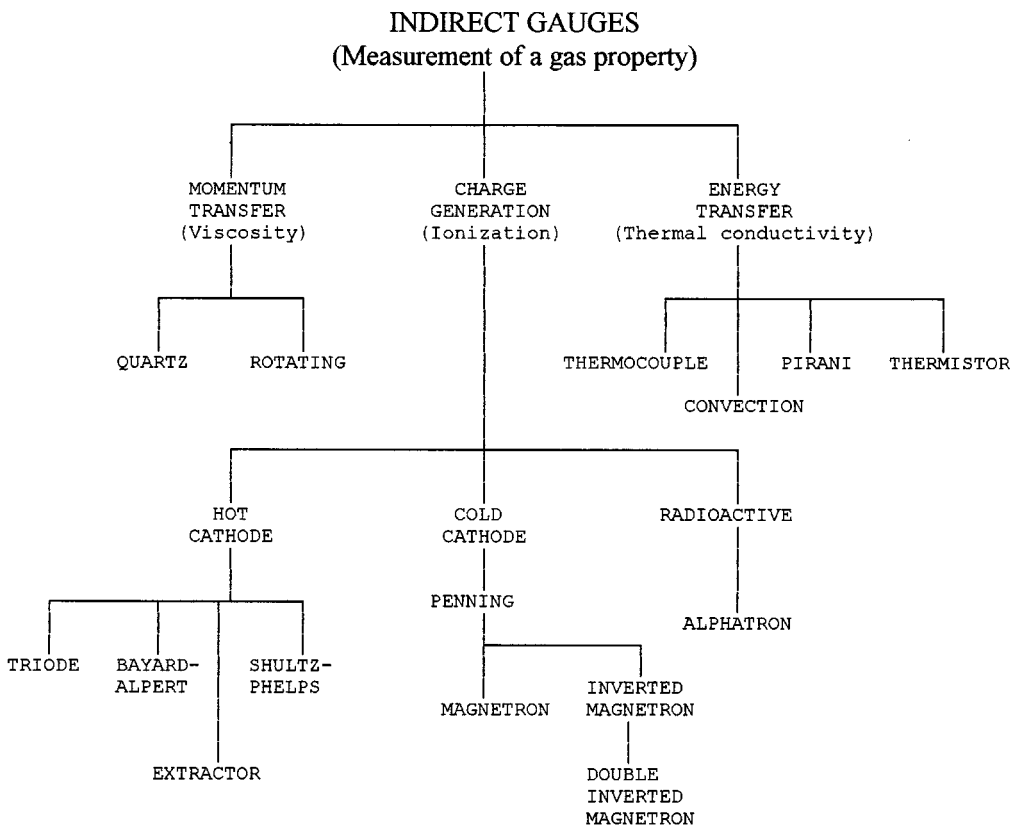
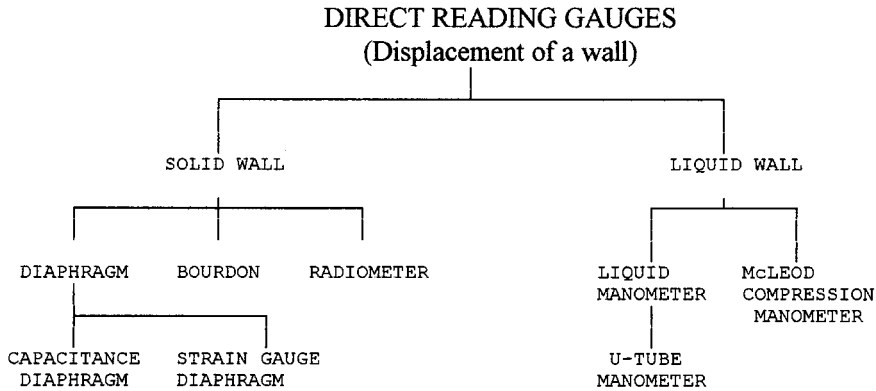


FIGURE 26.8 Classification of pressure gages. (From D.M. Hoffman, B. Singh, and J.H. Thomas, III (eds.), *The Handbook of Vacuum Science and Technology*, Orlando, FL: Academic Press, 1998. With permission.)

evacuated and sealed at one end and filled partly with mercury or a low vapor pressure liquid such as diffusion pump oil (See [Figure 26.10](#)). In the straight tube manometer, as the space above the mercury is evacuated, the length of the mercury column decreases. In the case of the U-tube, as the free end is evacuated, the two columns approach equal height. The pressure at the open end is measured by the difference in height of the liquid columns. If the liquid is mercury, the pressure is directly measured in mm of Hg (torr). The manometer is limited to pressures equal to or greater than ~1 torr (133 Pa). If

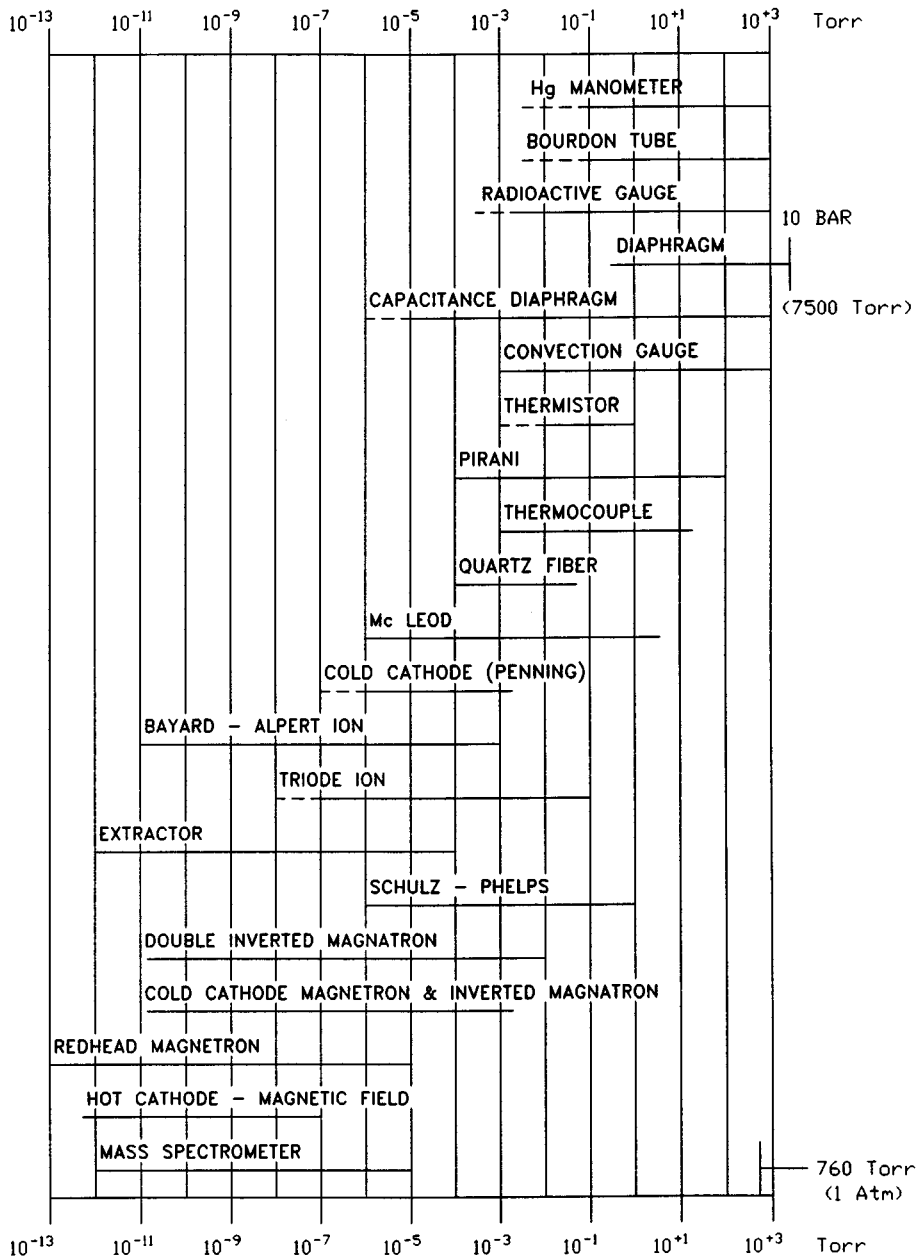


FIGURE 26.9 Pressure ranges for various gages. (From D.M. Hoffman, B. Singh, and J.H. Thomas, III (eds.), *The Handbook of Vacuum Science and Technology*, Orlando, FL: Academic Press, 1998. With permission.)

the liquid is a low density oil, the U-tube is capable of measuring a pressure as low as ~0.1 torr. This is an absolute, direct reading gage but the use of mercury or low density oils that will in time contaminate the vacuum system preclude its use as a permanent vacuum gage.

Due to the pressure limitation of the manometer, the McLeod gage [2, 3] was developed to significantly extend the range of vacuum measurement (see Figure 26.11). This device is essentially a mercury manometer in which a volume of gas is compressed before measurement. This can be used as a primary standard device when a liquid nitrogen trap is used on the vacuum system. Figure 26.11 shows gas at 10⁻⁶ torr and

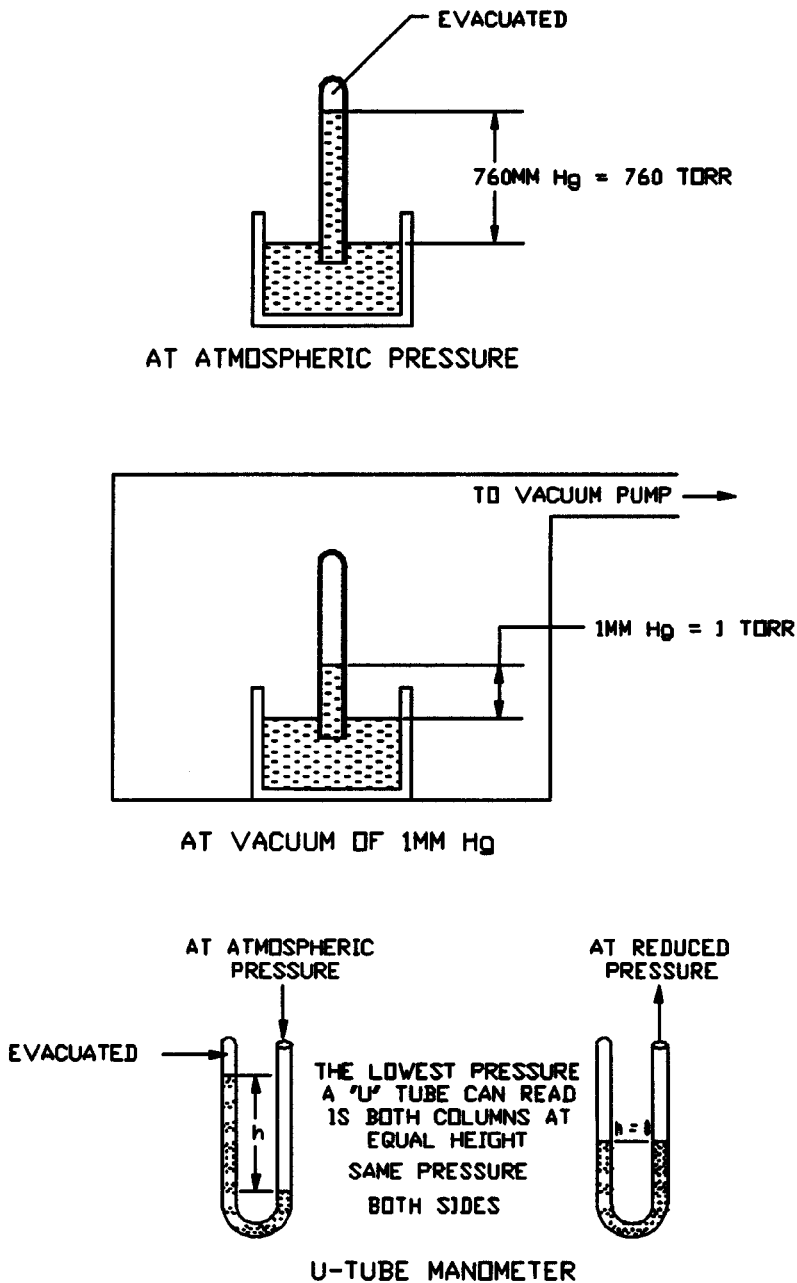


FIGURE 26.10 Mercury manometers. (From W.H. Bayles, Jr., Fundamentals of Vacuum Measurement, Calibration and Certification, Industrial Heating, October 1992. With permission.)

a compression ratio of 10^{+7} . In this example, the difference of the columns will be 10 mm. Extreme care must be taken not to break the glass and expose the surroundings to the mercury. The McLeod Gage is an inexpensive standard but should only be used by skilled and careful technicians. The gage will give a false low reading unless precautions are taken to ensure that any condensible vapors present are removed by liquid nitrogen trapping.

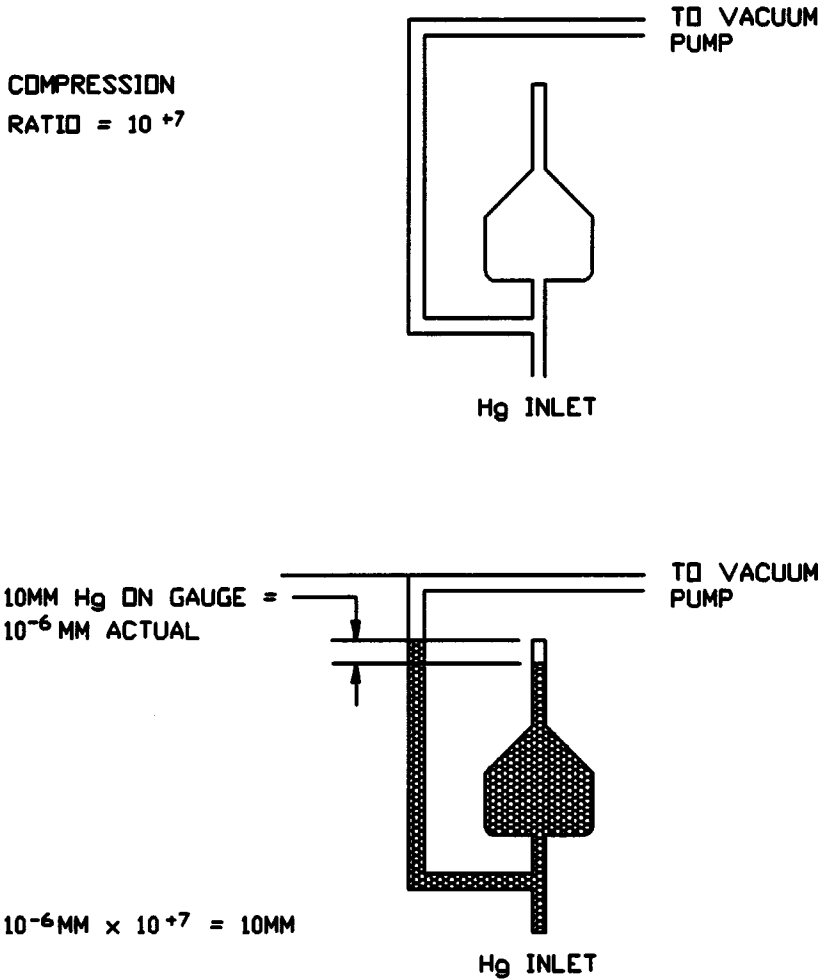


FIGURE 26.11 McLeod gage. (From D.M. Hoffman, B. Singh, and J.H. Thomas, III (eds.), *The Handbook of Vacuum Science and Technology*, Orlando, FL: Academic Press, 1998. With permission.)

Solid Wall Gages

There are two major mechanical solid wall gage types: capsule and diaphragm.

Bourdon Gages.

The capsule-type gages depend on the deformation of the capsule with changing pressure and the resultant deflection of an indicator. Pressure gages using this principle measure pressures above atmospheric to several thousand psi and are commonly used on compressed gas systems. This type of gage is also used at pressures below atmospheric, but the sensitivity is low. The Bourdon gage (Figure 26.12), is used as a moderate vacuum gage. In this case, the capsule is in the form of a thin-walled tube bent in a circle, with the open end attached to the vacuum system with a mechanism and a pointer attached to the other end. The atmospheric pressure deforms the tube; a linear indication of the pressure is given that is independent of the nature of the gas. Certain manufacturers supply capsule gages capable of measuring pressures as low as 1 torr. These gages are rugged, inexpensive, and simple to use and can be made of materials inert to corrosive vapors. Since changing atmospheric pressure causes inaccuracies in the readings, compensated versions of the capsule and Bourdon gage have been developed that improve the accuracy [4].

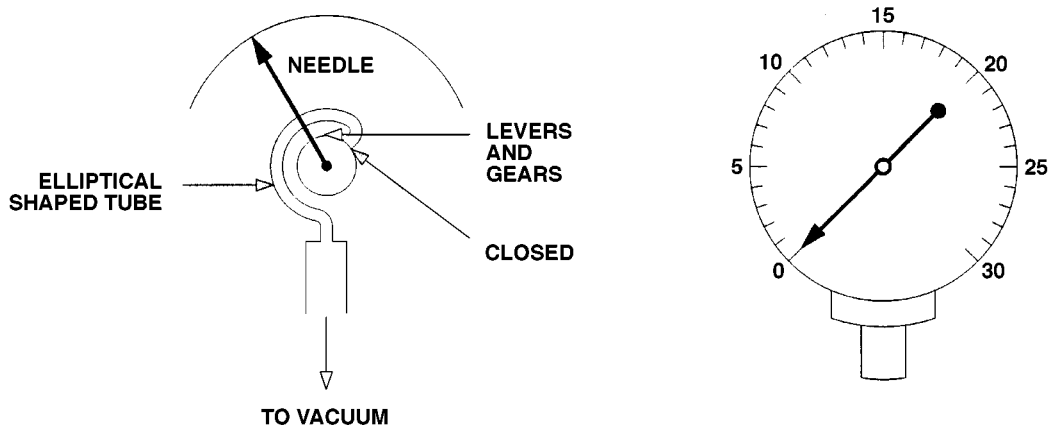


FIGURE 26.12 Bourdon gage. (From Varian Associates, Basic Vacuum Practice, Varian Associates, Inc., Lexington, MA, 1992. With permission.)

Diaphragm Gages.

If compensated capsule or diaphragm mechanisms are combined with sensitive and stable electronic measuring circuits, performance is improved. One such gage is the capacitance diaphragm gage (also referred to as the capacitance manometer).

The capacitance diaphragm gage is shown in Figure 26.13. A flexible diaphragm forms one plate of a capacitor and a fixed probe the other. The flexible diaphragm deforms due to even slight changes in pressure, resulting in a change in the capacitance. The capacitance is converted to a pressure reading. The sensitivity, repeatability, and simplicity of this gage enables this type of direct reading gage to be a standard from 10^{-6} torr to atmospheric pressure, provided multiple heads designed for each pressure range are used. A single head can have a dynamic range of 4 or 5 orders of magnitude [5].

The strain gage type of diaphragm gage is shown in Figure 26.13. In this case, deformation of the diaphragm causes a proportional output from the attached strain gage. Sensitivities and dynamic range tend to be less than those of the capacitance diaphragm gage, but the price of the strain gage type diaphragm gage is usually lower.

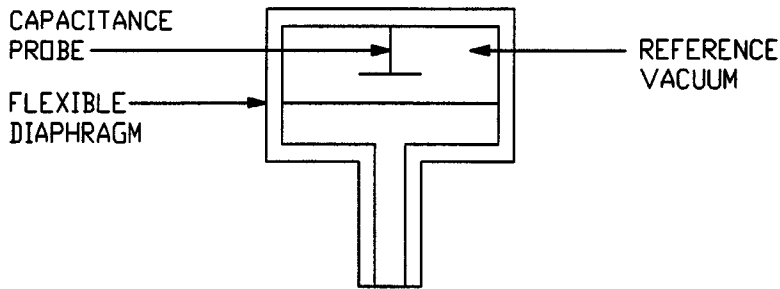
Both of these gages are prone to errors caused by small temperature changes due to the inherent high sensitivity of this gage type. Temperature-controlled heads or correction tables built into the electronics have been used to minimize this problem. Other sources of error in all solid wall gages are hysteresis and metal fatigue.

Indirect Reading Gages

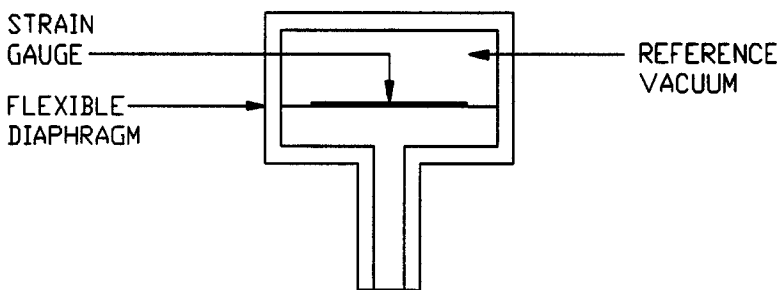
Indirect reading gages measure some property of the gas that changes with the density of the gas and usually produces an electric output. Electronic devices amplify and compensate this output to provide a pressure reading.

Thermal Conductivity Gages

Thermal conductivity gages utilize the property of gases in which reduced thermal conductivity corresponds to decreasing density (pressure). The thermal conductivity decreases from a nearly constant value above ~ 1 torr to essentially 0 at pressures below 10^{-2} torr. The gage controllers are designed to work with a specific sensor tube, and substitutions are limited to those that are truly functionally identical. Heat transfer at various pressures is related to the Knudsen number, as is shown in Figure 26.14 for various heat transfer regimes. The Knudsen number can then be related to pressure through the geometry of the sensor, providing a relationship of heat transfer to pressure for a particular design thermal conductivity gage.



CAPACITANCE DIAPHRAGM GAUGE



STRAIN GAUGE DIAPHRAGM GAUGE

FIGURE 26.13 Diaphragm gage. (From W.H. Bayles, Jr., *Fundamentals of Vacuum Measurement, Calibration and Certification*, Industrial Heating, October 1992. With permission.)

Pirani Gages.

The Pirani gage is perhaps the oldest indirect gage that is still used today. In operation, a sensing filament carrying current and producing heat is surrounded by the gas to be measured. As the pressure changes, the thermal conductivity changes, thus varying the temperature of the sensing filament. The temperature change causes a change in the resistance of the sensing filament. The sensing filament is usually one leg of a Wheatstone bridge. The bridge can be operated so that the voltage is varied to keep the bridge balanced; that is, the resistance of the sensing filament is kept constant.

This method is called the constant temperature method and is deemed the fastest, most sensitive, and most accurate. To reduce the effect of changing ambient temperature, an identical filament sealed off at very low pressure is placed in the leg adjacent to the sensing filament as a balancing resistor. Because of its high thermal resistance coefficient, the filament material is usually a thin tungsten wire. It has been demonstrated that a 10 W light bulb works quite well [6]. (see [Figure 26.15](#).)

A properly designed, compensated Pirani gage with sensitive circuitry is capable of measuring to 10^{-4} torr. However, the thermal conductivity of gases varies with the gas being measured, causing a variation in gage response. These variations can be as large as a factor of 5 at low pressures and as high as 10 at high pressures (see [Figure 26.16](#)). Correction for these variations can be made on the calibration curves supplied by the manufacturer if the composition of the gas is known. Operation in the presence of high partial pressures of organic molecules such as oils is not recommended.

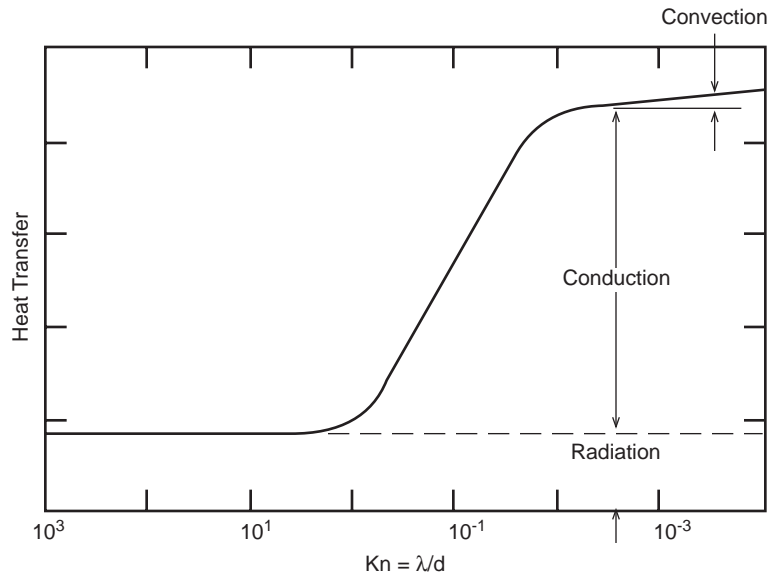


FIGURE 26.14 Heat transfer regimes in a thermal conductivity gage.

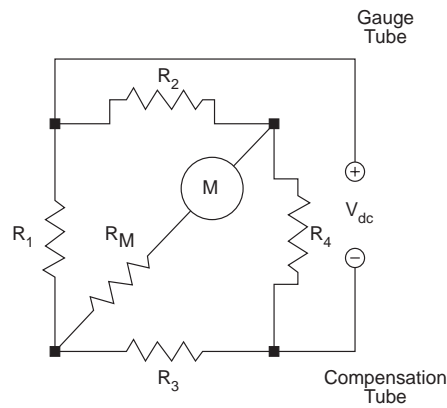


FIGURE 26.15 Pirani gage.

Thermistor Gages.

In the thermistor gage, a thermistor is used as one leg of a bridge circuit. The inverse resistive characteristics of the thermistor element unbalances the bridge as the pressure changes, causing a corresponding change in current. Sensitive electronics measure the current and are calibrated in pressure units. The

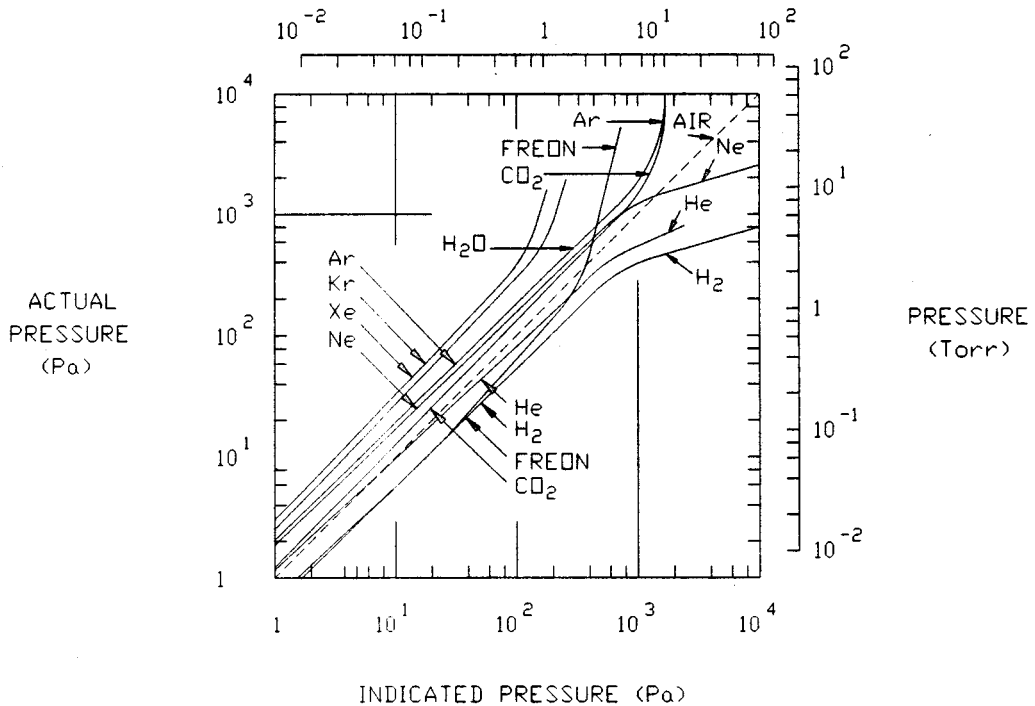


FIGURE 26.16 Calibration curves for the Pirani gage. (Reprinted with permission from Leybold-Herqeus GmbH, Köhn, Germany.)

thermistor gage measures approximately the same pressure range as the thermocouple. The exact calibration depends on the gas measured. In a well-designed bridge circuit, the plot of current vs. pressure is practically linear in the range 10^{-3} to 1 torr [7]. Modern thermistor gages use constant-temperature techniques.

Thermocouple Gages.

Another example of an indirect reading thermal conductivity gage is the thermocouple gage. This is a relatively inexpensive device with proven reliability and a wide range of applications. In the thermocouple gage, a filament of resistance alloy is heated by the passage of a constant current (see Figure 26.17). A thermocouple is welded to the midpoint of the filament or preferably to a conduction bridge at the center of the heated filament. This provides a means of directly measuring the temperature. With a constant current through the filament, the temperature increases as the pressure decreases as there are fewer molecules surrounding the filament to carry the heat away. The thermocouple output voltage increases as a result of the increased temperature and varies inversely with the pressure. The thermocouple gage can also be operated in the constant-temperature mode.

Gas composition effects apply to all thermal conductivity gages. The calibration curves for a typical thermocouple gage are shown in Figure 26.18. The thermocouple gage can be optimized for operation in various pressure ranges. Operation of the thermocouple gage in high partial pressures of organic molecules such as oils should be avoided. One manufacturer pre-oxidizes the thermocouple sensor for stability in “dirty” environments and for greater interchangeability in clean environments.

Convection Gages.

Below 1 torr a significant change in thermal conductivity occurs as the pressure changes. Thus, the thermal conductivity gage is normally limited to 1 torr.

At pressures above 1 torr, there is, in most gages, a small contribution to heat transfer caused by convection. Manufacturers have developed gages that utilize this convection effect to extend the usable

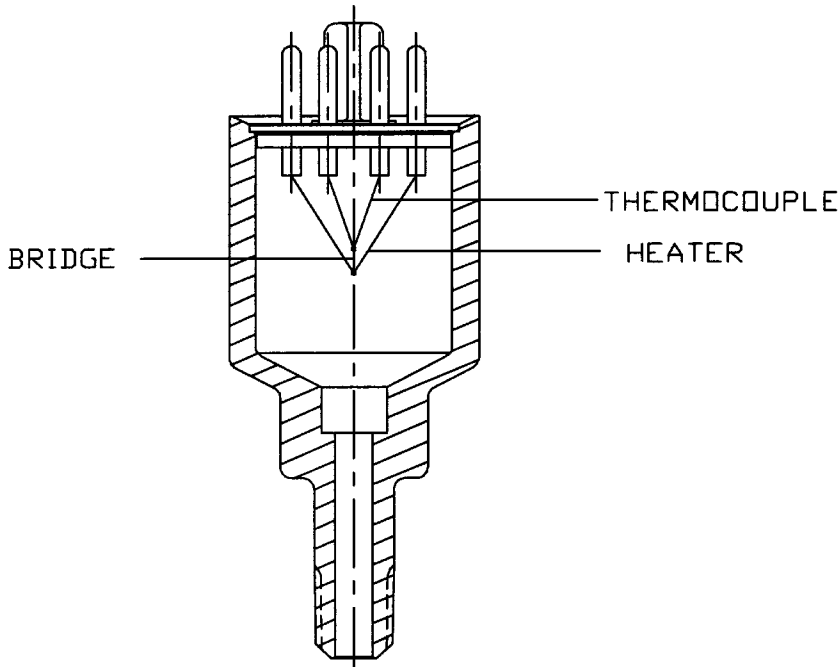


FIGURE 26.17 Thermocouple gage. (Reprinted with permission of Televac Division, The Fredericks Co., Huntingdon Valley, PA.)

range to atmospheric pressure and slightly above [8–12]. Orientation of a convection gage is critical because this convection heat transfer is highly dependent on the orientation of the elements within the gage.

The Convectron™ uses the basic structure of the Pirani with special features to enhance convection cooling in the high-pressure region [13]. To utilize the gage above 1 torr (133 Pa), the sensor tube must be mounted with its major axis in a horizontal position. If the only area of interest is below 1 torr, the tube can be mounted in any position. As mentioned above, the gage controller is designed to be used with a specific model sensor tube; because extensive use is made of calibration curves and look-up tables stored in the controller, no substitution is recommended.

The Televac convection gage uses the basic structure of the thermocouple gage except that two thermocouples are used [14]. As in any thermocouple gage, the convection gage measures the pressure by determining the heat loss from a fine wire maintained at constant temperature. The response of the sensor depends on the gas type. A pair of thermocouples is mounted a fixed distance from each other (see Figure 26.19). The one mounted lower is heated to a constant temperature by a variable current power supply. Power is pulsed to this lower thermocouple and the temperature is measured between heating pulses. The second (upper) thermocouple measures convection effects and also compensates for ambient temperature. At pressures below ~2 torr (270 Pa) the temperature in the upper thermocouple is negligible. The gage tube operates as a typical thermocouple in the constant-temperature mode. Above 2 torr, convective heat transfer causes heating of the upper thermocouple. The voltage output is subtracted from that of the lower thermocouple, thus requiring more current to maintain the wire temperature. Consequently, the range of pressure that can be measured (via current change) is extended to atmospheric pressure (see Figure 26.20). Orientation of the sensor is with the axis vertical.

The use of convection gages with process control electronics allows for automatic pump-down with the assurance that the system will neither open under vacuum nor be subject to over-pressure during backfill to atmospheric pressure. These gages, with their controllers, are relatively inexpensive. In oil-free systems, they afford long life and reproducible results.

METER
READING
(μm)

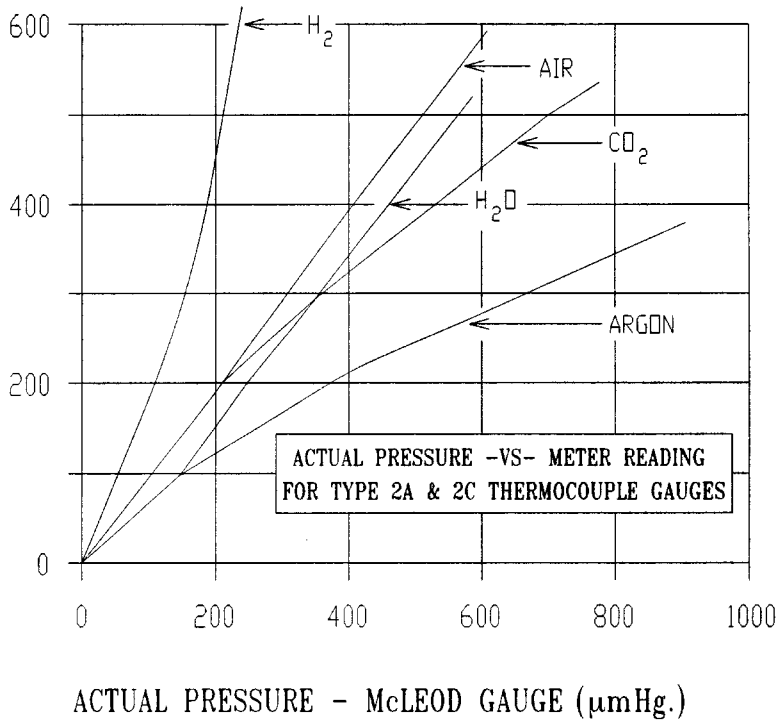


FIGURE 26.18 Calibration curves for the thermocouple gage. (Reprinted with permission from Televac Division, The Fredericks Co., Huntingdon Valley, PA.)

Hot Cathode Ionization Gages

Hot cathode ionization gage designs consist of triode gages, Bayard-Alpert gages, and others.

Triode Hot Cathode Ionization Gages.

For over 80 years, the triode electron tube has been used as an indirect way to measure vacuum [15, 16]. A typical triode connection is as an amplifier, as is shown in Figure 26.21. A brief description of its operation is given here, but more rigorous treatment of triode performance is given in [17–20]. However, if the triode is connected as in Figure 26.22 so that the grid is positive and the plate is negative with respect to the filament, then the ion current collected by the plate for the same electron current to the grid is greatly increased [21].

Today, the triode gage is used in this higher sensitivity mode. Many investigators have shown that a linear change in molecular density (pressure) results in a linear change in ion current [15, 21, 22]. This linearity allows a sensitivity factor S to be defined such that:

$$I_i = S \times I_e \times P \quad (26.3)$$

where I_i = Ion current (A)

I_e = Electron current (A)

P = Pressure

S = Sensitivity (in units of reciprocal pressure)

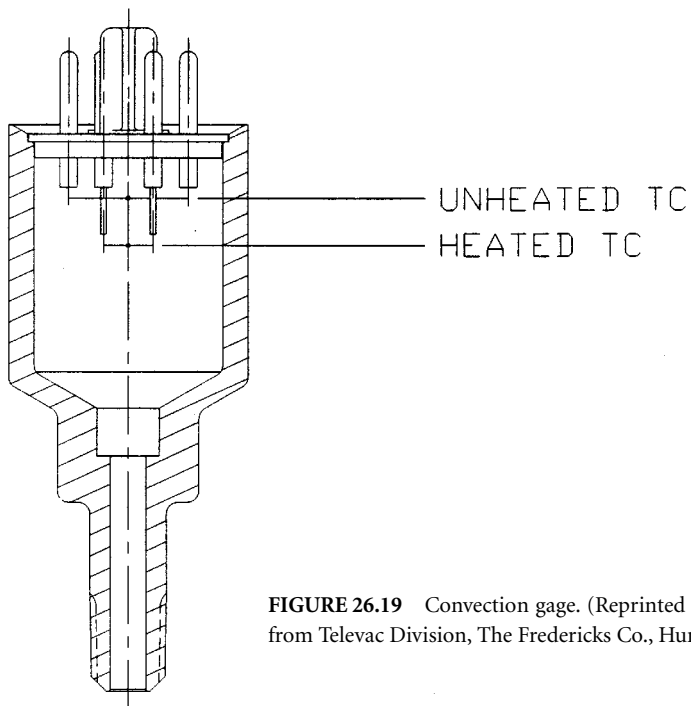


FIGURE 26.19 Convection gage. (Reprinted with permission from Televac Division, The Fredericks Co., Huntingdon Valley, PA.)

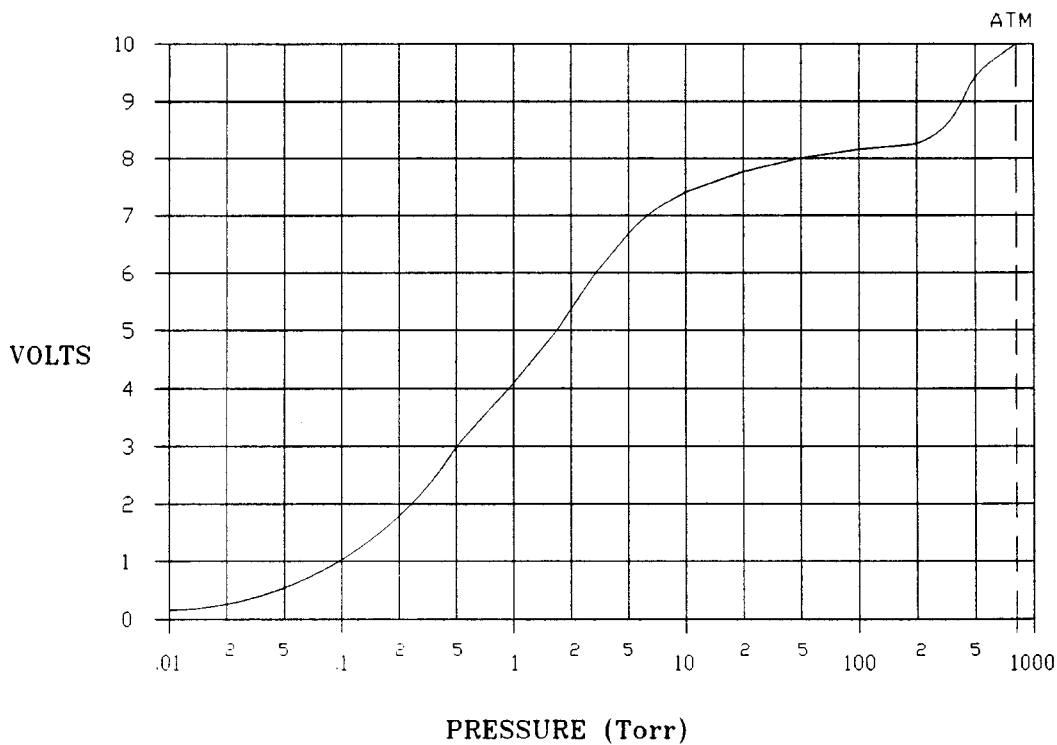


FIGURE 26.20 Output curve for the convection gage. (Reprinted with permission from Televac Division, The Fredericks Co., Huntingdon Valley, PA.)

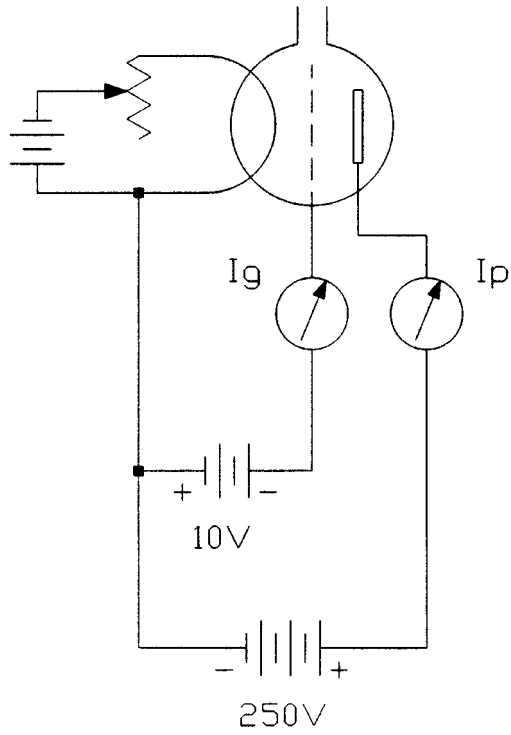


FIGURE 26.21 Typical triode connection.

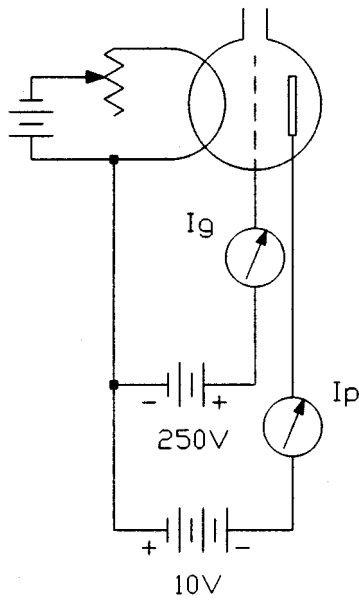


FIGURE 26.22 Alternative triode connection.

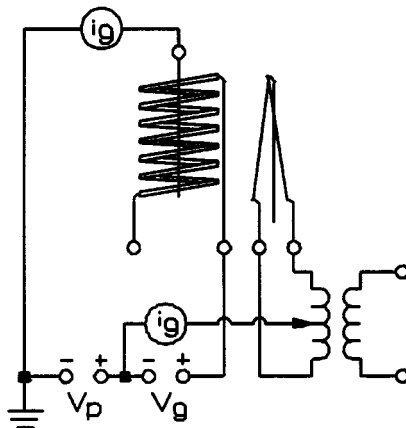
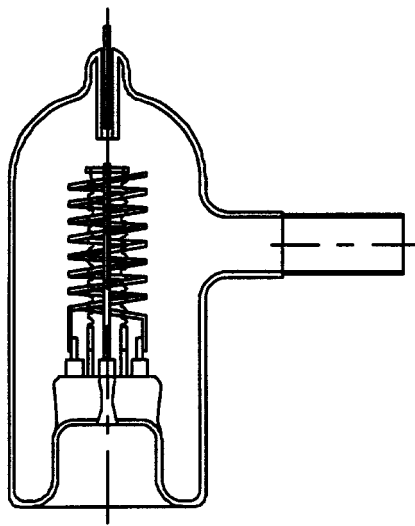


FIGURE 26.23 Bayard–Alpert hot cathode ionization gage.

Additional details are found in [23–25]. In nearly all cases, except at relatively high pressures, the triode gage has been replaced by the Bayard–Alpert gage.

Bayard–Alpert Hot Cathode Ionization Gages.

It became apparent that the pressure barrier observed at 10^{-8} torr was caused by a failure in measurement rather than pumping [26, 27]. A solution to this problem was proposed by Bayard and Alpert [28] that is now the most widely used gage for general UHV measurement.

The Bayard–Alpert gage is similar to a triode gage but has been redesigned so that only a small quantity of the internally generated X-rays strike the collector. The primary features of the Bayard–Alpert gage and its associated circuit are shown in Figures 26.23 and 26.24. The cathode has been replaced by a thin collector located at the center of the grid, and the cathode filament is now outside and several millimeters away from the grid. The Bayard–Alpert design utilizes the same controller as the triode gage, with

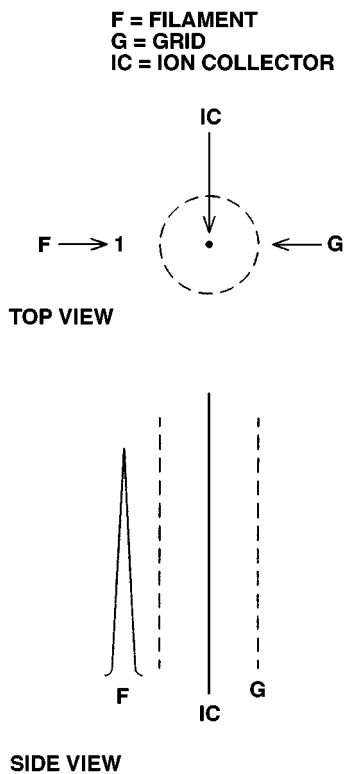


FIGURE 26.24 Bayard–Alpert gage configuration.

corrections for sensitivity differences between the gage designs. When a hot filament gage is exposed to high pressures, burn-out of the tungsten filaments often occurs. To prevent this, platinum metals were coated with refractory oxides to allow the gage to withstand sudden exposure to atmosphere with the filament hot [29, 30]. Typical materials include either thoria or yttria coatings on iridium. Bayard–Alpert and triode gages of identical structure and dimensions but with different filaments (i.e., tungsten vs. thoria iridium) were observed to have different sensitivities, with the tungsten filament versions being 20% to 40% more sensitive than the iridium of the same construction.

The lowest pressure that can be measured is limited by low energy X-rays striking the ion collector and emitting electrons. Several methods to reduce this X-ray limit were developed. Gage designs with very small diameter collectors have been made that extend the high vacuum range down to 10^{-12} torr, but accuracy was lost at the high pressures [31, 32].

The modulated gage was designed by Redhead [33] with an extra electrode near the ion collector. In this configuration, the X-ray current could be subtracted by measuring the ion current at two modulator potentials, thus increasing the range to 5×10^{-12} . Other gages use suppressor electrodes in front of the ion collector [34, 35].

The extractor gage (Figure 26.25) is the most widely used UHV hot cathode gage for those who need to measure 10^{-12} torr [36]. In this gage, the ions are extracted out of the ionizing volume and deflected or focused onto a small collector. More recent designs have been developed [37, 38]. The use of a channel electron multiplier [39] has reduced the low pressure limit to 10^{-15} torr.

The Bayard–Alpert gage suffers from some problems, however. The ion current is geometry dependent. Investigators have reported on the sensitivity variations, inaccuracy, and instability of Bayard–Alpert gages with widely differing results [40–46, 49, 50, 56]. Investigators have developed ways to reduce or eliminate some of these problems [47, 48].

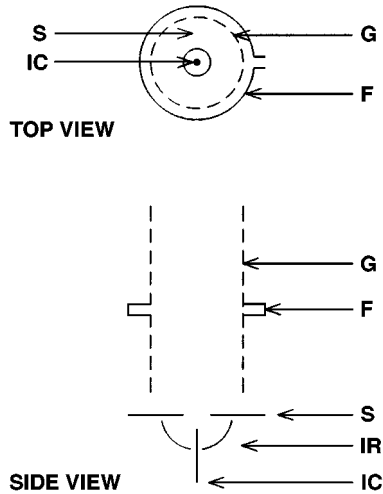


FIGURE 26.25 Extractor ionization gage. F, filament; G, grid; S, shield; IR, iron reflector; IC, ion collector.

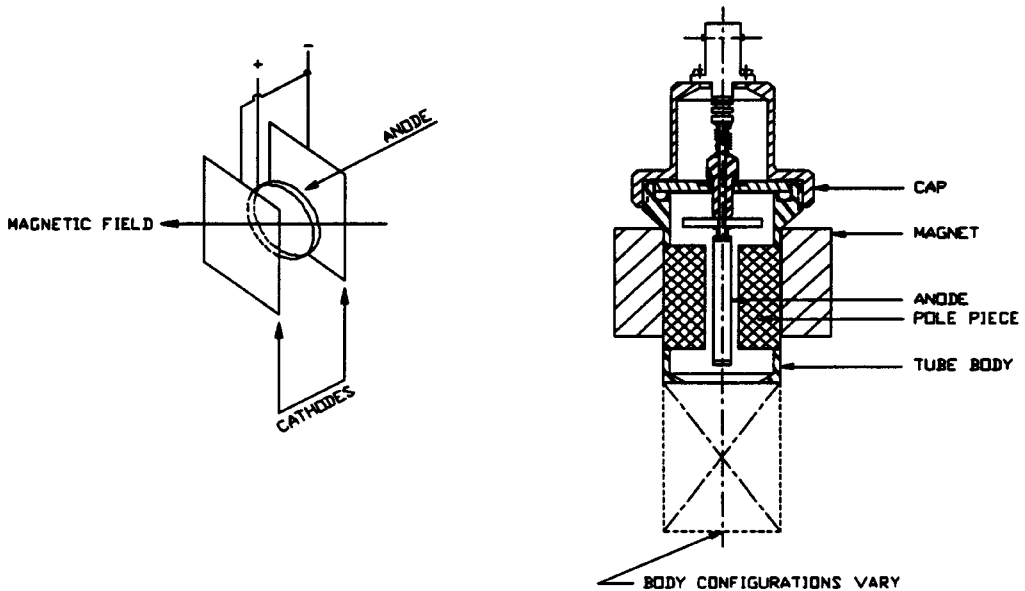


FIGURE 26.26 Penning gages. ([Left] From J.F. O'Hanlon, *A User's Guide to Vacuum Technology*, New York: John Wiley & Sons, 1980, 47. With permission. [Right] Reprinted with permission from Televac Division, The Fredericks Co., Huntingdon Valley, PA.)

Cold Cathode Ionization Gages

To measure pressures below 10^{-3} torr, Penning [51] developed the cold cathode discharge gage. Below 10^{-3} torr, the mean free path is so high that little ionization takes place. The probability of ionization was increased by placing a magnetic field parallel to the paths of ions and electrons to force these particles into helical trajectory.

This gage consists of two parallel cathodes and an anode, which is placed midway between them (see Figure 26.26). The anode is a circular or rectangular loop of metal wire whose plane is parallel to that of the cathodes. A few kilovolts potential difference is maintained between the anode and the cathodes.

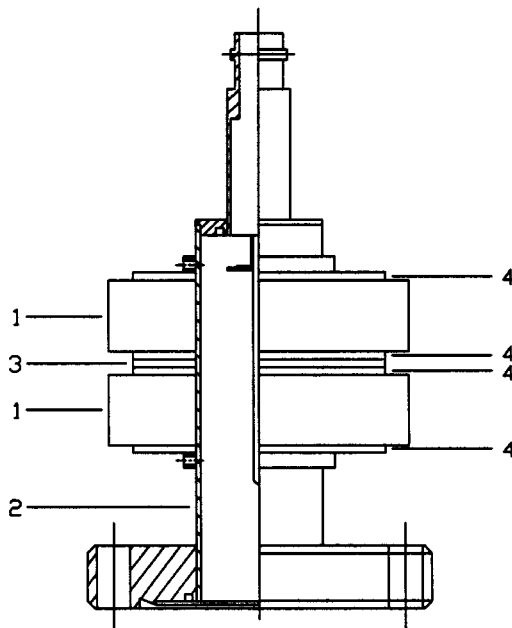


FIGURE 26.27 Double inverted magnetron. (Reprinted with permission from Televac Division, The Fredericks Co., Huntingdon Valley, PA.)

Furthermore, a magnetic field is applied between the cathodes by a permanent magnet usually external to the gage body. Electrons emitted from either of the two cathodes must travel in helical paths due to the magnetic field eventually reaching the anode, which carries a high positive charge. During the travel along this long path, many electrons collide with the molecules of the gas, thus creating positive ions that travel more directly to the cathodes. The ionization current thus produced is read out on a sensitive current meter as pressure.

This is a rugged gage used for industrial applications such as in leak detectors, vacuum furnaces, electron beam welders, and other industrial processes. The Penning gage is rugged, simple, and inexpensive. Its range is typically 10^{-3} torr to 10^{-6} torr, and some instability and lack of accuracy has been observed [52]. The magnetron design [53] and the inverted magnetron design [54] extended the low pressure range to 10^{-12} Torr [55] or better. These improvements produced a better gage but instability, hysteresis, and starting problems remain [57, 58]. Magnetrons currently in use are simpler and do not use an auxiliary cathode.

More recently, a double inverted magnetron was introduced [59]. This gage has greater sensitivity (amp/torr) than the other types (see Figure 26.27). It has been operated successfully at $\sim 1 \times 10^{-11}$ torr. The gage consists of two axially magnetized, annular-shaped magnets (1) placed around a cylinder (2) so that the north pole of one magnet faces the north pole of the other one. A nonmagnetic spacer (3) is placed between the two magnets and thin shims (4) are used to focus the magnetic fields. This gage has been operated to date at 10^{-11} torr, and stays ignited and reignites quickly when power is restored at this pressure. Essentially instantaneous reignition has been demonstrated by use of radioactive triggering [60].

Resonance Gages

One example of a resonance-type vacuum gage is the quartz friction vacuum gage [61]. A quartz oscillator can be built to measure pressure by a shift in resonance frequency caused by static pressure of the surrounding gas or by the increased power required to maintain a constant amplitude. Its range is from near atmospheric pressure to about 0.1 torr. A second method is to measure the resonant electrical impedance of a tuning fork oscillator. Test results for this device show an accuracy within $\pm 10\%$ for pressure from 10^{-3} torr to 10^3 torr. There is little commercial use to date for these devices.

Molecular Drag (Spinning Rotor) Gages

Meyer [62] and Maxwell [63] introduced the idea of measuring pressure by means of the molecular drag of rotating devices in 1875. The rotors of these devices were tethered to a wire or thin filament. The gage was further enhanced by Holmes [64], who introduced the concept of the magnetic rotor suspension, leading to the spinning rotor gage. Nearly 10 years later, Beams et al. [65] disclosed the use of a magnetically levitated, rotating steel ball to measure pressure at high vacuum. Fremerey [66] reported on the historical development of this gage.

The molecular drag gage (MDG), often referred to as the spinning rotor gage, received wider acceptance after its commercial introduction in 1982 [67]. It is claimed to be more stable than other gages at lower pressures [68].

The principle of operation of the modern MDG is based on the fact that the rate of change of the angular velocity of a freely spinning ball is proportional to the gas pressure and inversely proportional to the mean molecular velocity. When the driving force is removed, the angular velocity is determined by measuring the ac voltage induced in the pickup coils by the magnetic moment of the ball (see Figure 26.28).

In current practice, a small rotor (steel ball bearing) about 4.5 mm in diameter is magnetically levitated and spun up to about 400 Hz by induction. The ball, enclosed in a thimble connected to the vacuum system, is allowed to coast by turning off the inductive drive. Then, the time of a revolution of the ball is measured by timing the signal induced in a set of pickup coils by the rotational component of the ball's magnetic moment. Gas molecules will exert a drag on the ball, slowing it at a rate set by the pressure P , its molecular mass m , temperature T , and the coefficient of momentum transfer σ , between the gas and the ball. A perfectly smooth ball would have a value of unity. There is also a pressure-independent residual drag (RD) caused by eddy current losses in the ball and surrounding structure. There will also be temperature effects that will cause the ball diameter and moment of inertia to change.

The pressure in the region of molecular flow is given by:

$$P = \frac{\pi \rho a \bar{c}}{10 \sigma_{\text{eff}}} \left(\frac{-\omega' - \text{RD} - 2 \alpha T'}{\omega} \right) \quad (26.4)$$

Note: Some sources include the term $\frac{(8kT')}{(\pi m)}$

- where ρ = Density of the rotor
- a = Radius of the rotor
- ω'/ω = Fractional rate of slowing of the rotor
- \bar{c} = Mean gas molecular velocity
- α = Linear coefficient of expansion of the ball
- T' = Rate of change of the ball's temperature

All of the terms in the first part of the equation can be readily determined except for the accommodation coefficient σ , which depends on the surface of the ball and the molecular adhesion between the gas and the surface of the ball. The accommodation coefficient σ must be determined by calibration of the MDG against a known pressure standard or, if repeatability is more important than the highest accuracy, by assuming a value of 1 for σ . Measurements of σ on many balls over several years have been repeatedly performed by Dittman et al. [68]. The values obtained ranged from 0.97 to 1.06 for 68 visually smooth balls, so using a value of 1 for σ would not introduce a large error and would allow the MDG to be considered a primary standard (Fremerey [66]).

The controller [68] contains the electronics to power and regulate the suspension and drive, detect and amplify the signal from the pickup coils, and then time the rotation of the ball. It also contains a data processor that stores the calibration data and computes the pressure.

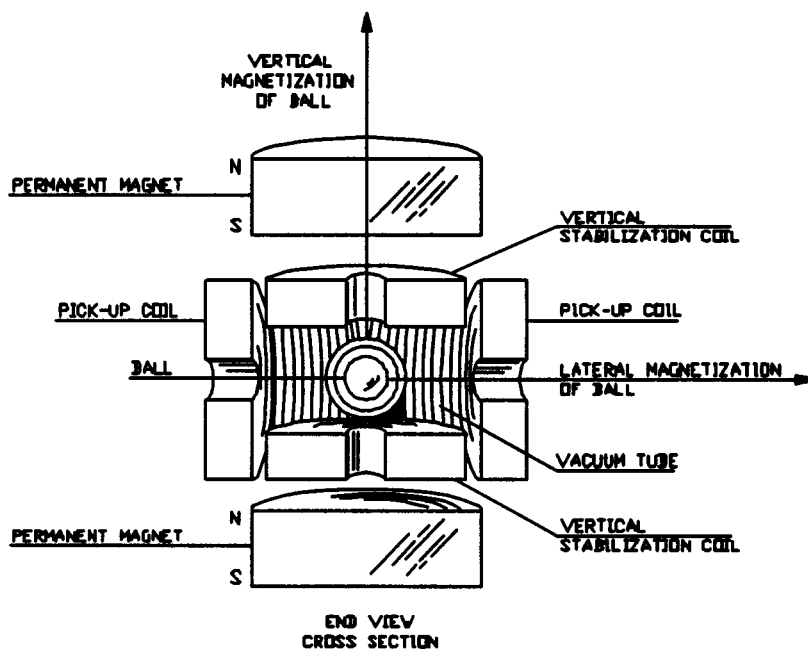
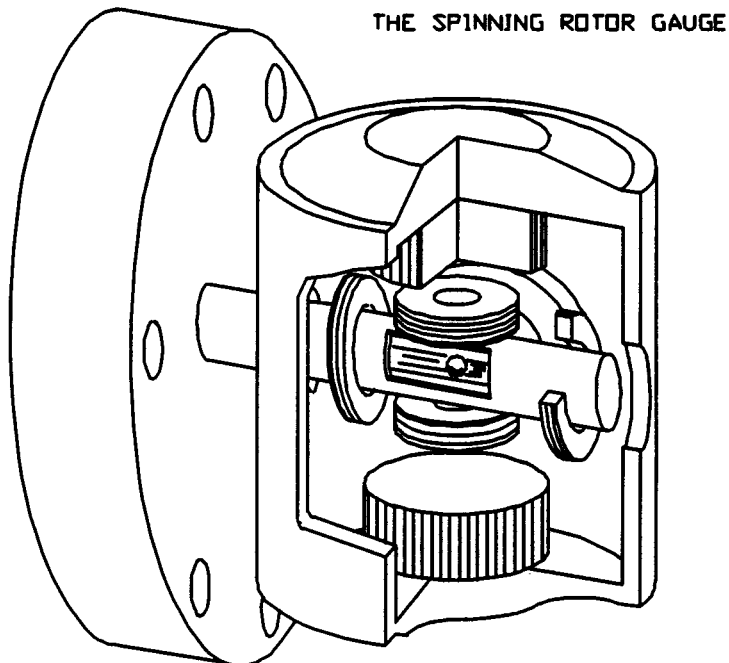


FIGURE 26.28 Molecular drag gage (spinning rotor).

The MDG is perhaps the best available transfer standard for the pressure range of 10^{-2} torr to 10^{-7} torr (1 Pa to 10^{-5} Pa) because it is designed for laboratory use in controlled, relatively vibration-free environments [69, 70].

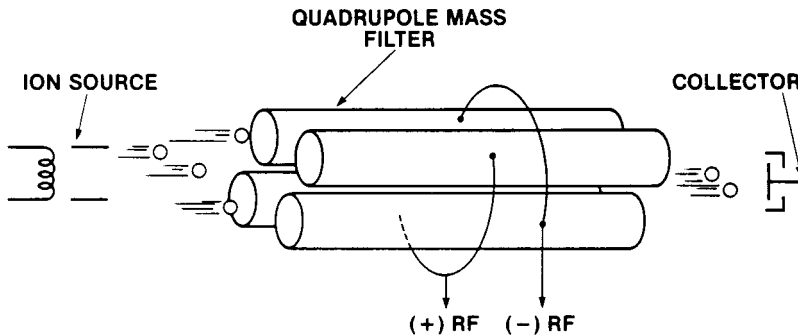


FIGURE 26.29 Quadrupole mass spectrometer. (From Varian Associates, Basic Vacuum Practice, Varian Associates, Inc., Lexington, MA, 1992. With permission.)

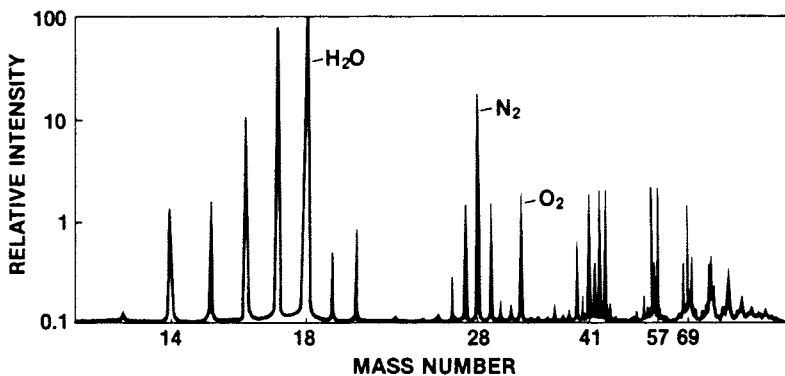


FIGURE 26.30 Relative intensity vs. mass number. (From Varian Associates, Basic Vacuum Practice, Varian Associates, Inc., Lexington, MA, 1992. With permission.)

Partial Pressure Measurements and Mass Spectrometers

The theory and practical applications of partial pressure measurements and mass spectrometers are discussed in detail in the literature [76]; however, an overview is presented herein [78].

A simple device for measuring the partial pressure of nitrogen as well as the total pressure in a vacuum system is the residual nitrogen analyzer (RNA). Operating in high vacuum, it is used to detect leaks in a vacuum system. It is effective because various gases are pumped at different rates and nitrogen is readily pumped, leaving a much lower percentage than is present at atmospheric pressure. Thus, the presence of a significant percentage of nitrogen at high vacuum indicates an air leak. The RNA consists of a cold cathode gage with an optical filter and a photomultiplier tube. Since ionization in the cold cathode tube produces light and the color is determined by the gases present, the RNA filters out all except for that corresponding to nitrogen and is calibrated to give the partial pressure of nitrogen.

A more complex device to measure the partial pressure of many gases in a vacuum chamber is the mass spectrometer-type residual gas analyzer (RGA). This device comes in many forms and several sizes. The quadrupole mass spectrometer is shown in Figure 26.29. The sensing head consists of an ion source, a quadrupole mass filter, and a Faraday cup collector. The quadrupole mass filter consists of two pairs of parallel rods having equal and opposite RF and dc voltages. For each combination of voltages, only ions of a specific mass will pass through the filter. The mass filter is tuned to pass only ions of a specific mass-to-charge ratio at a given time. As the tuning is changed to represent increasing mass numbers, a display such as Figure 26.30 is produced, showing the relative intensity of the signal vs. the mass number. This display can then be compared electronically with similar displays for known gases to determine the composition of the gases in the vacuum chamber. The head can operate only at high vacuum. However,

by maintaining the head at high vacuum and using a sampling technique, the partial pressures of gases at higher pressures can be determined.

Calibration of mass spectrometers can be accomplished by equating the integral (the total area under all the peaks, taking into account the scale factors) to the overall pressure as measured by another gage (cold cathode, BA, or MDG). Once calibrated, the mass spectrometer can be used as a sensitive monitor of system pressure. It is also important when monitoring system pressure to know what gases are present. Most gages have vastly different sensitivities to different gas species.

Additional references on the details of the MDG and other types of gages available and on calibration are found in the literature [69–73, 75, 76]. The material in this chapter was summarized from an article on the fundamentals of vacuum measurement, calibration, and certification [77] from the authors' contribution to *The Handbook of Vacuum Technology* [76] and from other referenced sources.

References

1. J.F. O'Hanlon, *A User's Guide to Vacuum Technology*, New York: John Wiley & Sons, 1980, 47.
2. H. McLeod, *Phil. Mag.*, 47, 110, 1874.
3. C. Engleman, Televac Div. The Fredericks Co. 2337 Philmont Ave., Huntingdon Valley, PA, 19006, private communication.
4. Wallace and Tiernan Div., Pennwalt Corp., Bellville, NJ.
5. R.W. Hyland and R.L. Shaffer, Recommended practices of calibration and use of capacitance diaphragm gage for a transfer standard, *J. Vac. Sci. Tech., A*, 9(6), 2843, 1991.
6. K.R. Spangenberg, *Vacuum Tubes*, New York: McGraw-Hill, 1948, 766.
7. S. Dushman, *Scientific Foundations of Vacuum Technique*, 2nd ed., J.M. Lafferty (ed.), New York: John Wiley & Sons, 1962.
8. W. Steckelmacher and B. Fletcher, *J. Physics E.*, 5, 405, 1972.
9. W. Steckelmacher, *Vacuum*, 23, 307, 1973.
10. A. Beiman, *Total Pressure Measurement in Vacuum Technology*, Orlando, FL: Academic Press, 1985.
11. Granville-Phillips, 5675 Arapahoe Ave., Boulder CO, 80303.
12. Televac Div. The Fredericks Co. 2337 Philmont Ave., Huntingdon Valley, PA, 19006.
13. Granville-Phillips Data Sheet 360127, 3/95.
14. Televac U.S. Patent No. 5351551.
15. O.E. Buckley, *Proc. Natl. Acad. Sci.*, 2, 683, 1916.
16. M.D. Sarbey, *Electronics*, 2, 594, 1931.
17. R. Champeix, *Physics and Techniques of Electron Tubes*, Vol. 1, New York: Pergamon Press, 1961, 154-156.
18. N. Morgulis, *Physik Z. Sowjetunion*, 5, 407, 1934.
19. N.B. Reynolds, *Physics*, 1, 182, 1931.
20. J.H. Leck, *Pressure Measurement in Vacuum Systems*, London: Chapman & Hall, 1957, 70-74.
21. S. Dushman and C.G. Found, *Phys. Rev.*, 17, 7, 1921.
22. E.K. Jaycock and H.W. Weinhart, *Rev. Sci. Instr.*, 2, 401, 1931.
23. G.J. Schulz and A.V. Phelps, *Rev. Sci. Instr.*, 28, 1051, 1957.
24. Japanese Industrial Standard (JIS-Z-8570), Method of Calibration for Vacuum Gages,
25. J.W. Leck, op. cit., 69.
26. W.B. Nottingham, *Proc. 7th Annu. Conf. Phys. Electron.*, M.I.T., Cambridge, MA, 1947.
27. H.A. Steinhertz and P.A. Redhead, *Sci. Am.*, March, 2, 1962.
28. R.T. Bayard and D. Alpert, *Rev. Sci. Instr.*, 21, 571, 1950.
29. O.A. Weinreich, *Phys. Rev.*, 82, 573, 1951.
30. O.A. Weinreich and H. Bleicher, *Rev. Sci. Instr.*, 23, 56, 1952.
31. H.C. Hseuh and C. Lanni, *J. Vac. Sci. Technol.*, A 5, 3244, 1987.
32. T.S. Chou and Z.Q. Tang, *J. Vac. Sci. Technol.*, A4, 2280, 1986.
33. P.A. Redhead, *Rev. Sci. Instr.*, 31, 343, 1960.

34. G.H. Metson, *Br. J. Appl. Phys.*, 2, 46, 1951.
35. J.J. Lander, *Rev. Sci. Instr.*, 21, 672, 1950.
36. P.A. Redhead, *J. Vac. Sci. Technol.*, 3, 173, 1966.
37. J. Groszkowski, *Le Vide*, 136, 240, 1968.
38. L.G. Pittaway, *Philips Res. Rept.*, 29, 283, 1974.
39. D. Blechshmidt, *J. Vac. Sci. Technol.*, 10, 376, 1973.
40. P.A. Redhead, *J. Vac. Sci. Technol.*, 6, 848, 1969.
41. S.D. Wood and C.R. Tilford, *J. Vac. Sci. Technol.*, A3, 542, 1985.
42. C.R. Tilford, *J. Vac. Sci. Technol.*, A3, 546, 1985.
43. P.C. Arnold and D.G. Bills, *J. Vac. Sci. Technol.*, A2, 159, 1984.
44. P.C. Arnold and J. Borichevsky, *J. Vac. Sci. Technol.*, A12, 568, 1994.
45. D.G. Bills, *J. Vac. Sci. Technol.*, A12, 574, 1994.
46. C.R. Tilford, A.R. Filippelli, et al., *J. Vac. Sci. Technol.*, A13, 485, 1995.
47. P.C. Arnold, D.G. Bills, et al., *J. Vac. Sci. Technol.*, A12, 580, 1994.
48. ETI Division of the Fredericks Co., Gage Type 8184.
49. T.A. Flaim and P.D. Owenby, *J. Vac. Sci. Technol.*, 8, 661, 1971.
50. J.F. O'Hanlon, op. cit., 65.
51. F.M. Pennin, *Physica*, 4, 71, 1937.
52. F.M. Penning and K. Nienhaus, *Philips Tech. Rev.*, 11, 116, 1949.
53. P.A. Redhead, *Can. J. Phys.*, 36, 255, 1958.
54. J.P. Hobson and P.A. Redhead, *Can. J. Phys.*, 33, 271, 1958.
55. NRC type 552 data sheet.
56. N. Ohsako, *J. Vac. Sci. Technol.*, 20, 1153, 1982.
57. D. Pelz and G. Newton, *J. Vac. Sci. Technol.*, 4, 239, 1967.
58. R.N. Peacock, N.T. Peacock, and D.S. Hauschulz, *J. Vac. Sci. Technol.*, A9, 1977 1991.
59. E. Drubetsky, D.R. Taylor, and W.H. Bayles, Jr., *Am. Vac. Soc., New Engl. Chapter, 1993 Symp.*
60. B.R. Kendall and E. Drubetsky, *J. Vac. Sci. Technol.*, A14, 1292, 1996.
61. M. Ono, K. Hirata, et al., Quartz friction vacuum gage for pressure range from 0.001 to 1000 torr, *J. Vac. Sci. Technol.*, A4, 1728, 1986.
62. O.E. Meyer, *Pogg. Ann.*, 125, 177, 1865.
63. J.C. Maxwell, *Phil. Trans. R. Soc.*, 157, 249, 1866.
64. F.T. Holmes, *Rev. Sci. Instrum.*, 8, 444, 1937.
65. J.W. Beams, J.L. Young, and J.W. Moore, *J. Appl. Phys.*, 17, 886, 1946.
66. J.K. Fremery, *Vacuum*, 32, 685, 1946.
67. NIST, Vacuum Calibrations Using the Molecular Drag Gage, Course Notes, April 15-17, 1996.
68. S. Dittman, B.E. Lindenau, and C.R. Tilford, *J. Vac. Sci. Technol.*, A7, 3356, 1989.
69. K.E. McCulloh, S.D. Wood, and C.R. Tilford, *J. Vac. Sci. Technol.*, A3, 1738, 1985.
70. G. Cosma, J.K. Fremery, B. Lindenau, G. Messer, and P. Rohl, *J. Vac. Sci. Technol.*, 17, 642, 1980.
71. C.R. Tilford, S. Dittman, and K.E. McCulloh, *J. Vac. Sci. Technol.*, A6, 2855, 1988.
72. S. Dittman, NIST Special Publication 250-34, 1989.
73. National Conference of Standards Laboratories, Boulder, CO.
74. M. Hirata, M. Ono, H. Hojo, and K. Nakayama, *J. Vac. Sci. Technol.*, 20(4), 1159, 1982.
75. H. Gantsch, J. Tewes, and G. Messer, *Vacuum*, 35(3), 137, 1985.
76. D.M. Hoffman, B. Singh, and J.H. Thomas, III (eds.), *The Handbook of Vacuum Science and Technology*, Orlando, FL: Academic Press, 1998.
77. W.H. Bayles, Jr., Fundamentals of Vacuum Measurement, Calibration and Certification, Industrial Heating, October 1992.
78. Varian Associates, Basic Vacuum Practice, Varian Associates, Inc., 121 Hartwell Ave., Lexington, MA 02173, 1992.

26.3 Ultrasound Measurement

Peder C. Pedersen

Applications of Ultrasound

Medical

Ultrasound has a broad range of applications in medicine, where it is referred to as *medical ultrasound*. It is widely used in obstetrics to follow the development of the fetus during pregnancy, in cardiology where images can display the dynamics of blood flow and the motion of tissue structures (referred to as real-time imaging), and for locating tumors and cysts. 3-D imaging, surgical applications, imaging from within arteries (intravascular ultrasound), and contrast imaging are among the newer developments.

Industrial

In industry, ultrasound is utilized for examining critical structures, such as pipes and aircraft fuselages, for cracks and fatigue. Manufactured parts can likewise be examined for voids, flaws, and inclusions. Ultrasound has also widespread use in process control. The applications are collectively called *Non-Destructive Testing* (NDT) or *Non-Destructive Evaluation* (NDE). In addition, *acoustic microscopy* refers to microscopic examinations of internal structures that cannot be studied with a light microscope, such as an integrated circuit or biological tissue.

Underwater

Ultrasound is likewise an important tool for locating structures in the ocean, such as wrecks, mines, submarines, or schools of fish; the term SONAR (SOund Navigation And Ranging) is applied to these applications.

There are many other usages of ultrasound that lie outside the scope of this handbook: ultrasound welding, ultrasound cleaning, ultrasound hyperthermia, and ultrasound destruction of kidney stones (lithotripsy).

Definition of Basic Ultrasound Parameters

Ultrasound refers to acoustic waves of frequencies higher than 20,000 cycles per second (20 kHz), equal to the assumed upper limit for sound frequencies detectable by the human ear. As acoustic waves fundamentally are mechanical vibrations, a medium (e.g., water, air, or steel) is required for the waves to travel, or propagate, in. Hence, acoustic waves cannot exist in vacuum, such as outer space. If a single frequency sound wave is produced, also termed a *continuous wave* (CW), the fundamental relationship between frequency, f , in Hz, the sound speed of the medium, c_0 , in m s^{-1} , and the wavelength, λ , in meters, is given as:

$$\lambda = \frac{c_0}{f} \quad (26.5)$$

The wavelength λ describes the length, in the direction of propagation, of one period of the sound wave. The wavelength determines, or influences, the behavior of many acoustic functions: The sound field emitted from an acoustic radiator (e.g., a transducer or loudspeaker) is determined by the radiator's size measured in wavelengths; the ability to differentiate between closely spaced reflectors is a function of the separation measured in wavelengths. Even when a sound pulse, rather than a CW sound, is transmitted, the wavelength concept is still useful, as the pulse typically contains a dominant frequency.

The vibrational activity on the surface of the sound source transfers the acoustic energy into the medium. If one were able to observe a very small volume, referred to as a *particle*, of the medium during transmission of sound energy, one would see the particle moving back and forth around a fixed position. Associated with the particle motion is an acoustic pressure, which refers to the pressure variation around the mean pressure (which is typically the atmospheric pressure). This allows the introduction of two important — and closely related — acoustic quantities: the *particle velocity*, $\vec{u}(\vec{r}, t)$, and the *acoustic pressure*, $p(\vec{r}, t)$. In this notation, the arrow above a symbol in bold indicates a vector. The symbol \vec{r} represents the position vector, which simply defines a specific location in space. Thus, both particle velocity and pressure are functions of three spatial variables, x , y , and z , and the time variable, t .

To characterize a medium acoustically, the most important parameter is the *specific acoustic impedance*, z . For a lossless medium, z is given as follows:

$$z = \rho_0 c_0 \quad (26.6)$$

In Equation 26.6, ρ_0 is the density of the medium, measured in kg m^{-3} . When a medium absorbs acoustic energy (which all media do to a greater or smaller extent), the expression for acoustic impedance also contains a small imaginary term; this will be ignored in the discussions presented in this chapter. The acoustic impedance relates the particle velocity to the acoustic pressure:

$$z = \frac{p(\vec{r}, t)}{u(\vec{r}, t)} \quad (26.7)$$

Note that the relationship in Equation 26.7 uses the scalar value of the particle velocity (a scalar is a quantity, such as temperature, that does not have a direction associated with it). Equation 26.7 is exact for plane wave fields and a very good approximation for arbitrary acoustic fields. In a plane wave, all points in a plane normal to (i.e., which forms a 90° angle with respect to) the direction of propagation have the same pressure and particle velocity.

The acoustic impedances on either side of an interface (boundary between different media) determine the acoustic pressure reflected from the interface. Let a plane wave traveling in a medium with the acoustic impedance z_1 encounter a planar, smooth interface with another medium having the acoustic impedance z_2 . Assume that the plane wave propagates directly toward the interface; this is commonly referred to as insonification under normal incidence. In this case, the pressure and the intensity reflection coefficients, R and R_I , respectively, are as follows:

$$R = \frac{p_r}{p_i} = \frac{z_2 - z_1}{z_2 + z_1} \quad (26.8)$$

$$R = \frac{I_r}{I_i} = \left(\frac{z_2 - z_1}{z_2 + z_1} \right)^2$$

Intensity is a measure of the mean power transmitted through unit area and is measured in watts per square meter. The corresponding pressure and intensity transmission coefficients, T and T_I , respectively, are:

$$T = \frac{p_t}{p_i} = \frac{2z_2}{z_2 + z_1} \quad (26.9)$$

$$T_I = \frac{I_t}{I_i} = \frac{4z_1z_2}{(z_2 + z_1)^2}$$

The subscripts “i,” “r,” and “t” in Equations 26.8 and 26.9 refer to incident, reflected, and transmitted, respectively. The expressions in these two equations can be considered approximately valid for nonplanar waves under near-normal incidence. However, when the incident angle (angle between direction of propagation and the normal to the surface) becomes large, the reflection and transmission coefficients can change dramatically. In addition, the reflected and transmitted signals will also change if the surface is rough to the extent that the rms (root mean square) height exceeds a few percent of the wavelength.

The wave propagation can take several forms. In fluids and gases, only *longitudinal* (or *compressional*) waves exist, meaning that the direction of wave propagation is equal to the direction of the particle velocity vector. In solids, both longitudinal and *shear* waves exist which propagate in different directions and with different sound speeds. Transverse waves can exist on strings where the particle motion is normal to the direction of propagation. (Strictly speaking, shear waves can propagate a short distance in liquids [fluids] if the viscosity is sufficiently high.)

Conceptual Description of Ultrasound Imaging and Measurements

Most ultrasound measurements are based on the generation of a short ultrasound pulse that propagates in a specified direction and is partly reflected wherever there is an abrupt change in the acoustic properties of the medium and detection of the resulting echoes (pulse-echo ultrasound). A change in properties can be due to a cyst in liver tissue, a crack in a high-pressure pipe, or reflection from layers in the sea bottom. The degree to which a pulse is reflected at an interface is determined by the change in acoustic impedance as described in Equation 26.8. An image is formed by mapping echo strength vs. travel time (proportional to distance) and beam direction, as illustrated in [Figure 26.31](#). This is referred to as *B-mode* imaging (Brightness-mode). Further signal processing can be applied to compensate for attenuation (the damping out of the pressure pulse as it propagates) of the medium or to control focusing. Signal processing can also be applied to analyze echoes for information about the structure of materials or about the surface characteristics of rough surfaces.

A block diagram of a simplified pulse-echo ultrasound measurement system is shown in [Figure 26.32](#). The pulser circuit can generate a large voltage spike for exciting the transducer in B-mode applications, or the arbitrary function source can produce a short burst for Doppler measurements, or a coded waveform, such as a linear sweep. The amplifier brings the driving voltage to a level where the transducer can generate an adequate amount of acoustic energy.

The transducer is made from a piezoelectric ceramic that has the property of producing mechanical vibrations in response to an applied voltage pulse and generating a voltage when subjected to mechanical stress. When an image is required, the transducer can be a mechanical sector probe that produces a fan-shaped image by means of a single, mechanically steered, focused transducer element. Alternatively, the transducer can be a linear array transducer (described later) that produces a rectangular image. In the case of an array transducer, the pulser/amplifier must contain a driving circuit for each element in the array, in addition to delay control. To achieve a short pulse and good sensitivity, the transducer is equipped with backing material and matching layers (to be discussed later).

The receiver block contains a low-noise amplifier with time-varying gain to correct for medium attenuation and often a circuit for logarithmic compression. In the case of array transducers, the receiver circuitry is a complex system of amplifiers, time-varying delay elements, and summing circuits. The signal processing block can be part analog and part digital. The echo signals are envelope detected and digitized; the *envelope* of a signal is a curve that follows the amplitude of the received signal. A scan converter changes the signal into a format suitable for display on a gray-scale monitor. Information about ultrasound pulser-receiver instrumentation for NDE measurements can be found in [1] and for medical imaging in [2].

Not all ultrasound measurement systems are based on the pulse-echo concept. For material characterization, *transmission measurements* are frequently used, as illustrated in [Figure 26.33](#). The main difference between the pulse-echo system and the transmission system is that two transducers are used in the transmission system; the description of the individual blocks for the pulse-echo system applies generally here also. Imaging is generally not possible, although tomographic imaging of either attenuation

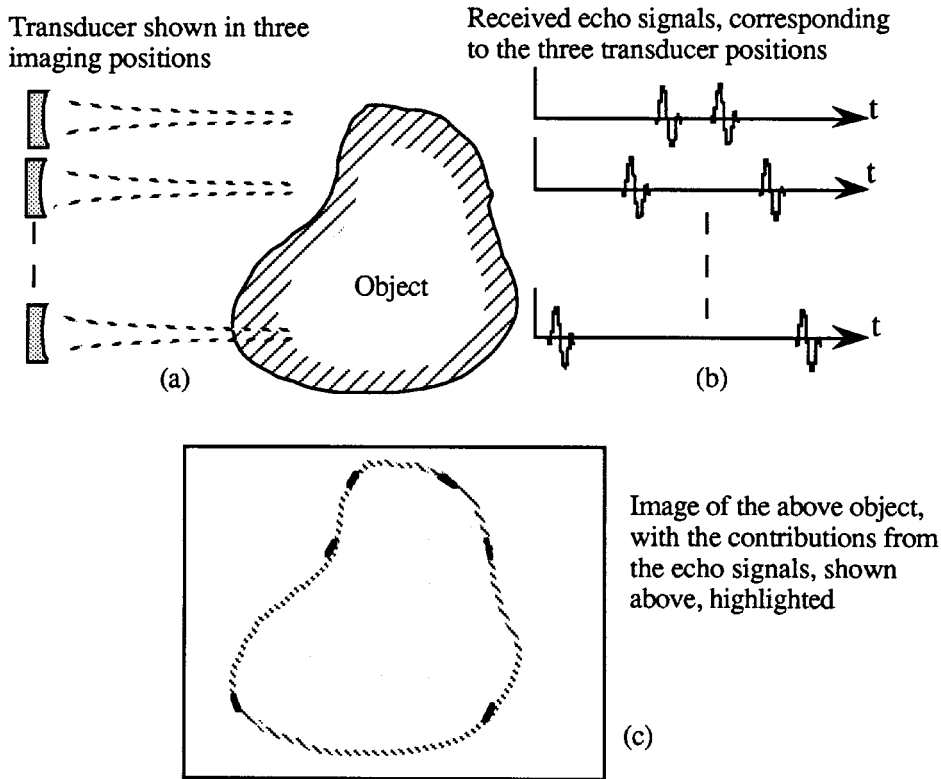


FIGURE 26.31 (a) A focused transducer insonifies the irregular object from different positions out of which only three are shown. The different transducer positions can readily be obtained by the use of an array transducer (to be described later). (b) Received echoes from the front and back of the object are displayed vs. travel time. It is here assumed that the structure is only weakly reflecting and that the attenuation has only a minimal effect. (c) An image is formed, based on the echo strengths and the echo arrival times.

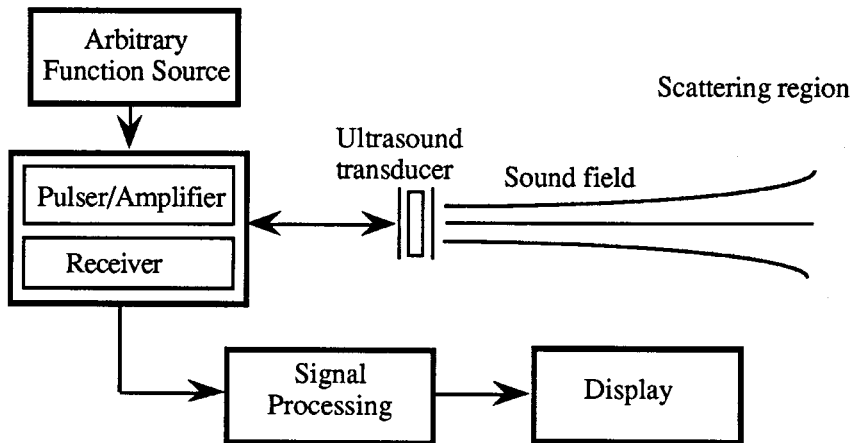


FIGURE 26.32 Simplified block diagram of a pulse-echo ultrasound system.

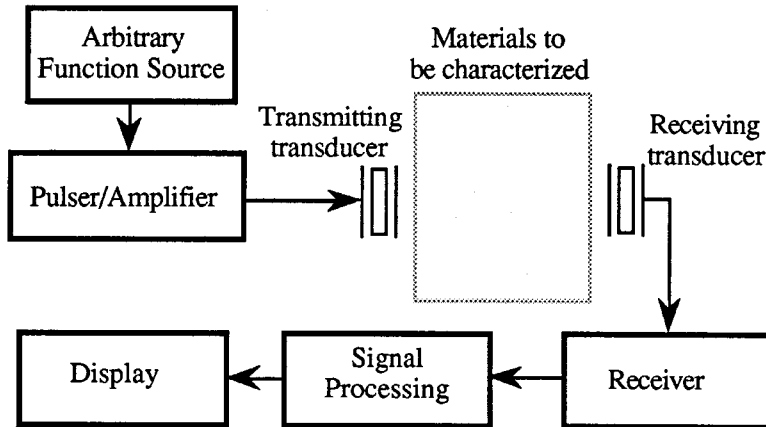


FIGURE 26.33 Simplified block diagram of ultrasound transmission system.

or velocity has been attempted. If the two transducers are moved together, voids and inclusions located in the transmission path can be detected.

Transmission measurements require, of course, that the structure or the medium of interest is accessible from opposite sides. This system allows accurate characterization of the attenuation and the sound speed of the medium from which a variety of material properties can be derived. Flow in a pipe or a channel can also be determined with a transmission system, by determining the difference between upstream and downstream propagation times.

Single-Element and Array Transducers

The device that converts electric energy into acoustic energy and vice versa is termed the *transducer* or, more specifically, the ultrasound transducer. Piezoelectric ceramics can be used for all frequencies in the ultrasound range; however, for ultrasound frequencies in the 20 kHz to 200 kHz range, magnetostrictive devices are occasionally used, which are based on materials that exhibit mechanical deformation in response to an applied magnetic field. Ultrasound transducers are commercially available for many applications over a wide range of frequencies.

Single-element transducers are used for basic measurements and material characterization, while array transducers with many individual transducer elements are used for imaging purposes. The former type costs from a few hundreds dollars and up, whereas the latter type costs in the thousands of dollars and requires extensive electronics for beam control and signal processing. A third alternative is the mechanical sector scanner where a single transducer is mechanically rotated over a specified angle. A single-element transducer consists of a piezoelectric element, a backing material that enables the transducer to respond to a fairly wide range of frequencies (but with reduced sensitivity), and a matching layer and faceplate that provide improved coupling into the medium and protect the transducer.

Although broadband transducers are very desirable, the energy conversion characteristics of the practical transducer correspond to that of a bandpass filter, i.e., the ultrasound pulse has most of its energy distributed around one frequency. This is the frequency referred to when, for example, one orders a 3.5 MHz transducer. The 6 dB bandwidth can be from 50% to 100% of the transducer frequency; the 6 dB bandwidth is the frequency range over which the transducer can produce an acoustic pressure that is at least 50% of the acoustic pressure at the most efficient frequency. The radiation characteristics of a transducer are determined by the geometry of the transducer (square, circular, plane, focused, etc.) and by the dimensions measured in wavelengths. Hence, a 10 MHz transducer tends to be smaller than a 5 MHz transducer. Focusing can also be achieved by means of an acoustic lens.

Array transducers exist in three main categories: phased arrays, linear arrays, and annular arrays. A fourth category could exist commercially in a few years: the 2-D array or a sparse 2-D array. Common for these array transducers is the fact that *during transmission*, the excitation time and excitation signal amplitude for each transducer element are controlled independently. This allows the beam to be steered in a given direction, as well as focused at a given point in space. *During reception*, an independently controlled time delay — which may be time varying — can be applied to each element before summation with the signal from other elements. The delay control permits the transducer to have maximal sensitivity to an echo from a specified range, and, moreover, to shift this point in space away from the transducer as echoes from structures further away are received. A limitation of the phased and linear arrays is that beam steering and focusing can only take place within the image plane. In the direction normal to the image plane, a fixed focus is produced by the physical shape of the array elements.

The phased array transducer consists of a fairly small number of elements, such as 16 to 32. Both beam steering and focusing are carried out, producing a pie-shaped image. The phased array is most suitable when only a narrow observation window exists, as is the case when imaging the heart from the space between the ribs. The linear array transducer has far more elements, typically between 128 and 256. It activates only a subset of all the elements for a given measurement, and produces focusing, but generally not beam steering, so that the beam direction is normal to the array surface. Consider a linear array transducer with 128 elements, labeled 1 to 128. If one assumes that the first pulse-echo measurement is made with elements 1 to 16, the next measurement with elements 2 to 17, etc., the beam will have been *linearly* translated along the long dimension of the linear array (hence the name), producing a rectangular image format. The annular array transducer consists of a series of concentric rings. As such, it cannot steer the beam, but can focus both in transmit and receive mode, just as the phased and linear arrays. Thus, the annular array transducer is not suitable for imaging unless the transducer is moved mechanically. Its specific advantage is uniform focusing.

Selection Criteria for Ultrasound Frequencies

The discussion so far has often mentioned *frequency* as an important variable, without providing any guidance as to what ultrasound frequencies should be used. There is generally no technological limitation with respect to choice of ultrasound frequency, as frequencies even in the gigahertz (GHz, 10^9 Hz) range can be produced. The higher the frequency, the better is the control over the direction and the width of the ultrasound beam, leading to improved axial and lateral resolution. However, the attenuation increases with higher frequency. For many media, the attenuation varies with the frequency squared; while for biological soft tissue, the attenuation varies nearly linearly with frequency.

Generally, the ultrasound frequency is chosen as high as possible while still allowing a satisfactory signal-to-noise ratio (SNR) of the received signal. This rule does not always hold; for example, for grain size estimation in metals and for rough surface characterization, the optimal frequency has a specific relationship to the mean grain dimension or the rms roughness.

Basic Parameters in Ultrasound Measurements

Ultrasound technology today has led to a very wide range of applications, and the following overview mentions only the basic parameters. For an in-depth review, see [3]. A discussion of applications is given at the end of the Ultrasound Theory and Applications section.

Reflection (or Transmission) Detected or Not

The most basic measurement consists of determining whether a reflected or transmitted signal is received or not. This can be used to monitor liquid level where the absence of liquid prevents ultrasound transmission from taking place, or to detect the existence of bubbles in a liquid (e.g., for dialysis purposes, where the bubbles are the reflectors) or for counting objects, such as bottles, on a conveyer belt.

Travel Time

Travel time is the elapsed time from transmission of an ultrasound pulse to the detection of a received pulse in either a pulse-echo or a transmission system. If the sound speed is known, the thickness of an object can be found from the time difference between the front surface echo and the back surface echo. Conversely, sound speed can be determined when the thickness is known. By measuring with a broadband pulse (a short pulse containing a broad range of frequencies), velocity dispersion (frequency dependence of velocity) can be found, which has applications for materials characterization. Elastic parameters can also be found from velocity measurements. Imaging applications are generally made based on the assumption of a known, constant velocity; thus, round-trip travel times from the transducer to the reflecting structures and back in a known direction gives the basis for the image formation.

Attenuation

The attenuation and its frequency dependence are important materials parameters, as they can be used to differentiate between normal and pathological biological tissue, measure porosity of ceramics, the grain size of metals, and the structure of composite materials. Attenuation can be found by means of transmission measurements by determining the signal amplitude with the test object first absent and then present; here, transmission losses must also be considered, as quantified in Equation 26.9. Attenuation can be obtained from pulse-echo measurements, by comparing the strength of echoes from the front and back surfaces of the specimen under test. Diffraction effects (described later in the *Advanced Topics in Ultrasound* section) might need to be considered. Attenuation can be considered as a bulk parameter for the medium as a whole, or it can be determined for small regions of the medium.

Reflection Coefficient

The strength of a reflection at an interface between two media is determined by the change in acoustic impedance across the interface, as shown in Equation 26.8. This allows, at least in principle, the impedance of one medium to be determined from the measured reflection coefficient and the impedance of the other medium. In fact, the term *impediography* refers to the determination of the impedance profile of a layered medium by means of this concept. In practice, the measurement is not easy to carry out, as the transducer must be aligned very accurately at normal incidence to the medium surface. By measuring the reflection coefficient vs. incident angle at a planar, smooth surface, a velocity estimate of the reflecting medium can be made; in an alternative application, reflection measurements vs. frequency permit the evaluation of rough surface parameters.

Parameters Obtained Through Signal Processing

A number of object parameters can be obtained from analysis of the received signals. Material properties can be extracted from speckle analysis (analysis of statistical fluctuations in the image) and other forms of statistical analysis. Recognition of objects with complex shapes can, in some cases, be done by extracting specific features of the received signals. Doppler processing for velocity estimation is another example of information that is only attainable by means of signal processing. By combining several “stacked” images, 3-D reconstruction is possible, from which volume estimation and rate of change of volume are possible, such as for determining the dynamics of the left ventricle of the heart.

Ultrasound Theory and Applications

Sound Velocity

The propagation speed, c_0 , is generally determined by the density and the elastic properties of the medium. For an ideal gas, c_0 may be expressed as [4]:

$$c_0 = \sqrt{\gamma P_0 / \rho_0} = \sqrt{\gamma r T_K} \quad (26.10)$$

where $\gamma = C_p/C_v$, the ratio of specific heats; for air, $\gamma = 1.402$. P_0 is the static pressure of the gas, which at 1 atm is $1.013 \times 10^5 \text{ N m}^{-2}$. ρ_0 is the specific density of the gas, equal to 1.293 kg m^{-3} for air at 1 atm and 0°C . The constant r is the ratio of the universal gas constant and the molecular weight of the gas, and T_K is the temperature in kelvin. Substituting the values for air into the first equation in Equation 26.10 gives $c_0 = 331.6 \text{ m s}^{-1}$ at 0°C . As the ratio P_0/ρ_0 is constant for varying pressure, but constant temperature, c_0 is likewise pressure independent. (For a real gas, c_0 exhibits, in fact, a small dependence on pressure.)

The temperature dependence of an ideal gas can be obtained by rewriting the second expression in Equation 26.10 as follows

$$c_0 = c_{\text{ref}} \sqrt{1 + T/273} \quad (26.11)$$

where c_{ref} is the sound speed at 0°C , and T is the temperature in $^\circ\text{C}$.

In liquids, the expression for c_0 is given as

$$c_0 = \sqrt{K_s/\rho_0} \quad (26.12)$$

where K_s is the adiabatic bulk modulus. Expressions for actual liquids as a function of temperature and pressure are not easily derived, and are often empirically determined. For pure water, the sound speed as a function of temperature and pressure can be given as:

$$c_{\text{H}_2\text{O}} = 1402.4 + 5.01T - 0.055T^2 + 0.00022T^3 + 1.6 \times 10^{-6} P_0 \quad (26.13)$$

In Equation 26.13, T is temperature in $^\circ\text{C}$, and P_0 is the static pressure in N m^{-2} ; the expression is valid for a pressure range from 1 atm to 100 atm.

Finally, for solids, the sound speed for longitudinal waves, c_L , is [5]:

$$c_L = \left(\frac{c_{11}}{\rho_0} \right)^{1/2} = \left(\frac{\lambda + 2\mu}{\rho_0} \right)^{1/2} \quad (26.14)$$

In Equation 26.14, c_{ij} is the the elastic stiffness constant, such that c_{11} refers to longitudinal stress over longitudinal strain, and $\lambda = c_{12}$ and $\mu = c_{44}$ are the Lamé elastic constants.

Wave Propagation in Homogeneous Media

In order to effectively use ultrasound for measurement purposes, it is essential to be able to describe the behavior of acoustic fields. This includes the general behavior, and maybe even a detailed understanding, of the radiated field from ultrasound transducers; the transmission, reflection, and refraction of an acoustic field at boundaries and layers; and the diffraction of of acoustic field at finite-sized reflectors.

The wave equation is a differential equation that formulates how an acoustic disturbance (acoustic pressure or particle velocity) propagates through a homogeneous medium. For an arbitrary wave field, the wave equation takes the following general form:

$$\nabla^2 p = \frac{1}{c^2} \frac{\partial^2 p}{\partial t^2} \quad (26.15)$$

where ∇^2 is the Laplacian operator. Equation 26.15 is also valid when particle velocity is substituted for pressure. If the condition of a plane wave field at a single frequency (also called a harmonic plane wave field) is imposed, the solution to Equation 26.15 is:

$$p(\vec{r}, t) = A \exp\left[j(\omega t - \vec{k} \times \vec{r})\right] + B \exp\left[j(\omega t + \vec{k} \times \vec{r})\right] \quad (26.16)$$

In Equation 26.16, $p(\vec{r}, t)$ consists of a plane wave propagating in the direction defined by the propagation vector \vec{k} and a plane wave in the direction $-\vec{k}$. As before, \vec{r} is a position vector that, in a Cartesian coordinate system, can be expressed as $\vec{r} = x\hat{x} + y\hat{y} + z\hat{z}$ where \hat{x} , \hat{y} , and \hat{z} are unit vectors. The magnitude of \vec{k} is called the wavenumber:

$$k = \omega/c_0 = 2\pi/\lambda \quad (26.17)$$

Expressing \vec{k} in the Cartesian coordinate system gives:

$$\vec{k} = k_x\hat{x} + k_y\hat{y} + k_z\hat{z} \quad (26.18)$$

When k , k_x , and k_y are specified, k_z is defined as well:

$$k_z = \sqrt{\left(\left(\omega/c_0\right)^2 - k_x^2 - k_y^2\right)} \quad (26.19)$$

Applying the expressions for \vec{r} and \vec{k} to Equation 26.16 and considering only the plane wave in the direction of $+\vec{k}$ gives

$$p(\vec{r}, t) = A \exp\left[j\left(\omega t - (k_x x + k_y y + k_z z)\right)\right] \quad (26.20)$$

From Equation 26.20, one sees that the amplitude of a plane wave is constant and equal to A , but that the phase varies with both time and space. When the direction of \vec{k} is specified, k_x , k_y , and k_z are found from projection onto the coordinate axes.

Solving Equation 26.15 under the assumption of spherical waves at a single frequency, with the source placed at the origin of the coordinate system, gives:

$$p(r, t) = \frac{A}{r} \exp\left[j(\omega t - kr)\right] + \frac{B}{r} \exp\left[j(\omega t + kr)\right] \quad (26.21)$$

The first term is a diverging spherical wave, and the second term is a converging spherical wave. The reason that the vector dot product does not appear in Equation 26.21 is that \vec{k} and \vec{r} always point in the same direction for spherical waves. While Equation 26.21 gives the complete solution, in most cases only a diverging spherical wave exists. If spherical waves are produced by a spherical source of radius a , then:

$$p(r, t) = \frac{A}{r} \exp\left[j(\omega t - kr)\right], \quad r > a \quad (26.22)$$

Acoustic Intensity and Sound Levels

The acoustic intensity, I , describes the mean power transported through a unit area normal to the direction of propagation. A general expression for I for a CW pressure function is:

$$I = \frac{1}{T} \int_0^T p(t)u(t) dt \quad (26.23)$$

In Equation 26.23, T represents one full cycle of the pressure function, and $u(t)$ is the particle velocity function. For a plane wave, the intensity is:

$$I = \frac{P^2}{2\rho_0 c_0} = \frac{1}{2}PU \quad (26.24)$$

where P and U are the magnitudes of the pressure and the particle velocity functions, respectively. The expression for I in Equation 26.24 can also be used as an approximation for nonplanar waves, such as spherical waves, as long as (kr) is large.

The intensity levels for pulse-echo measurements are often described by the SPTA (*Spatial Peak, Temporal Average*) value, which therefore refers to the mean intensity at the point in space where the intensity is the highest. Although the guidelines for exposure levels for medical imaging, set by the FDA, vary for different parts of the body, a general upper limit is 100 mW cm^{-2} . Given that the duty cycle (pulse duration/pulse interval) is typically in the order of 0.0001 for ultrasound imaging, the temporal peak intensity is much higher, and is even approaching the level where nonlinear effects can begin to be observed. Intensity levels used for NDE are application dependent, but are generally in the same range as in medical ultrasound.

Sound levels are logarithmic expressions (expressions in dB) of the pressure level or the intensity level. The term SPL stands for sound pressure level and is given as:

$$\text{SPL} = 20 \log \left(\frac{P_e}{P_{\text{ref}}} \right) \quad [\text{dB}] \quad (26.25)$$

In Equation 26.25, P_e is the effective pressure of the acoustic wave and P_{ref} is the reference effective pressure. Correspondingly, IL is the intensity level defined as:

$$\text{IL} = 10 \log \left(\frac{I}{I_{\text{ref}}} \right) \quad [\text{dB}] \quad (26.26)$$

where I_{ref} is the reference acoustic intensity.

Several reference levels are commonly used [6]. In air, $P_{\text{ref}} = 20 \text{ }\mu\text{Pa}$ and $I_{\text{ref}} = 10^{-12} \text{ W m}^{-2}$ are nearly equivalent reference levels. For water, typical pressure reference levels are $P_{\text{ref}} = 1 \text{ }\mu\text{Pa}$, $P_{\text{ref}} = 20 \text{ }\mu\text{Pa}$ or $P_{\text{ref}} = 1 \text{ }\mu\text{bar} = 0.1 \text{ Pa}$, with corresponding intensity reference levels of $I_{\text{ref}} = 6.76 \times 10^{-19} \text{ W m}^{-2}$, $I_{\text{ref}} = 2.70 \times 10^{-16} \text{ W m}^{-2}$, and $I_{\text{ref}} = 6.76 \times 10^{-9} \text{ W m}^{-2}$.

Wave Propagation Across Layers and Boundaries

The reflection and transmission coefficients for a plane wave impinging at normal incidence on the interface between two half spaces were given in Equations 26.8 and 26.9. It is also important to consider the transmission and reflection of waves at non-normal incidence and across a layer.

When a longitudinal wave impinges at a liquid–liquid interface, both the transmitted and the reflected waves are longitudinal waves, as illustrated in [Figure 26.34\(a\)](#). However, when a longitudinal wave propagating in a liquid medium encounters a liquid–solid interface under oblique incidence, both a longitudinal and a shear transmitted wave and a longitudinal reflected wave will result, as shown in [Figure 26.34\(b\)](#). The change of direction of the transmitted waves relative to the incident wave is referred to as *refraction*, which is caused by the difference in sound speed between the two media.

The magnitude and direction of the reflected and transmitted waves are determined by two simple boundary conditions: (1) the *pressure* on both sides of the boundary must be equal at all times, and (2) the *normal particle velocity* on both sides of the boundary must be equal at all times; the normal particle velocity refers to the component of the particle velocity that is normal to the boundary.

The boundary conditions lead to the following two relationships:

$$\sin \theta_i = \sin \theta_r ; \quad \frac{\sin \theta_i}{c_1} = \frac{\sin \theta_t}{c_2} \quad (26.27)$$

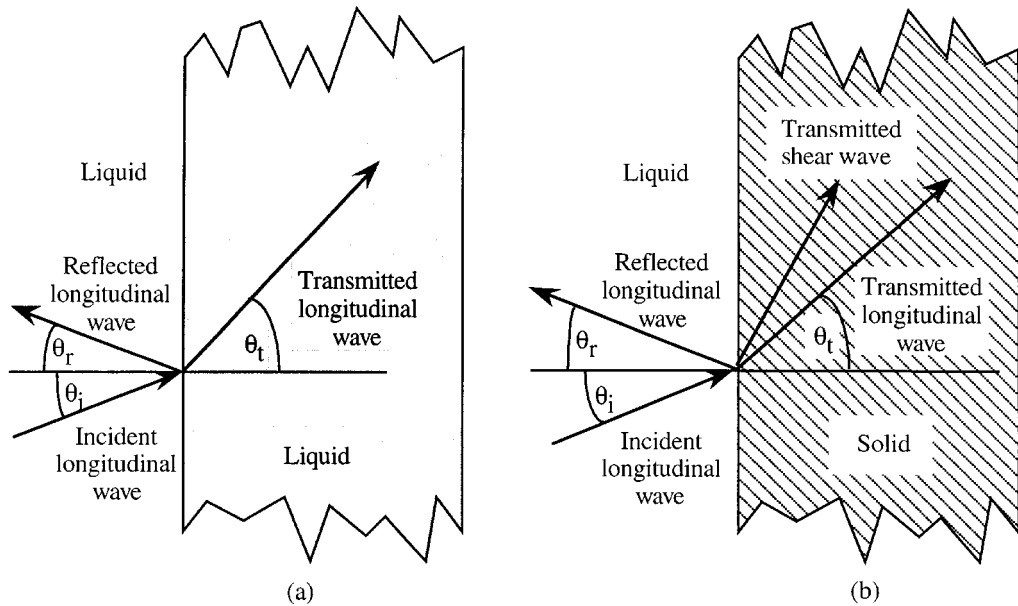


FIGURE 26.34 (a). An incident longitudinal wave at a liquid–liquid interface produces a reflected and a transmitted longitudinal wave. (b) An incident longitudinal wave at a liquid–solid interface produces a reflected longitudinal wave, transmitted longitudinal, and shear waves. The incident, reflected, and transmitted angles are indicated.

where c_1 and c_2 are the sound speeds of the two media, and θ_i , θ_r , and θ_t are the incident, reflected and transmitted angles, respectively. From Equation 26.27, one sees that

$$\theta_r = \theta_i; \quad \theta_t = \arcsin\left(\frac{c_2}{c_1} \sin\theta_i\right) \quad (26.28)$$

The second expression in Equation 26.28 is referred to as Snell’s law and quantifies the degree of refraction. Refraction affects the quality of ultrasound imaging because image formation is based on the assumption that the ultrasound beam travels in a straight path through all layers and inhomogeneities, and that the sound speed is constant throughout the medium. When the actual beam travels along a path that deviates to some extent from a straight path and passes through some parts of the medium faster than it does other parts, the resulting image is a distorted depiction of reality. Correcting this distortion is a very complex problem and, in the near future, one should only expect image improvement in the simplest cases.

It can be seen from Equation 26.28 that angle θ_t is not defined if the argument to the arcsin function exceeds unity. This defines a critical incident angle as follows:

$$\sin\theta_c = \frac{c_1}{c_2} \quad (26.29)$$

at or above which the reflection coefficient is 1 and the transmission coefficient is 0. A critical angle only exists when $c_1 < c_2$. The transmitted shear and longitudinal velocities each correspond to a different critical angle of incidence.

From the boundary conditions, the reflection coefficient as a function of incident angle can be determined [7]:

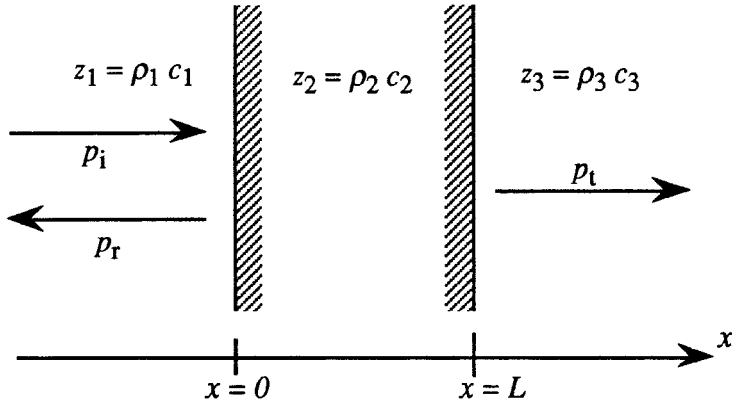


FIGURE 26.35 A pressure wave is incident on a layer of thickness L and with acoustic impedance $z_2 = \rho_2 c_2$.

$$R(\theta_i) = \frac{\left(\frac{z_2}{z_1}\right) - \left(\frac{\cos \theta_t}{\cos \theta_i}\right)}{\left(\frac{z_2}{z_1}\right) + \left(\frac{\cos \theta_t}{\cos \theta_i}\right)}, \text{ where } \cos \theta_t = \sqrt{1 - \left(\frac{c_2}{c_1}\right)^2 \sin^2 \theta_i} \quad (26.30)$$

The result in Equation 26.30 is referred to as the Rayleigh reflection coefficient.

The transmission of plane waves under normal incidence through a single layer is often of interest. The dimensions and the medium parameters are defined in Figure 26.35.

By applying the boundary conditions to both interfaces of the layer, both reflection and transmission coefficients are obtained [7], as given in Equations 26.31 and 26.32.

$$R = \frac{P_r}{P_i} = \frac{\left(1 - z_1/z_3\right) \cos k_2 L + j\left(z_2/z_3 - z_1/z_2\right) \sin k_2 L}{\left(1 + z_1/z_3\right) \cos k_2 L + j\left(z_2/z_3 + z_1/z_2\right) \sin k_2 L} \quad (26.31)$$

$$T = \frac{P_t}{P_i} = \frac{2}{\left(1 + z_1/z_3\right) \cos k_2 L + j\left(z_2/z_3 + z_1/z_2\right) \sin k_2 L} \quad (26.32)$$

A number of special conditions for Equation 26.31 can be considered, such as: (1) $z_1 = z_3$, which simplifies the numerator in Equation 26.31; and (2) the layer thickness is only a small fraction of a wavelength, that is, $k_2 L \ll 1$ which makes $\cos k_2 L \approx 1$ and $\sin k_2 L \approx k_2 L$. One case is of particular interest: the choice of thickness and acoustic impedance for the layer that makes $R = 0$, and therefore gives 100% energy transmission. This is fulfilled for:

$$k_2 L = \pi/2 + n\pi; \quad z_2 = \sqrt{z_1 z_3} \quad (26.33)$$

The result in Equation 26.33 states that the layer must be a quarter of a wavelength thick (plus an integer number of half wavelengths) and must have an acoustic impedance that is the geometric mean of the impedances of the media on either side. Among several applications of the *quarter wavelength impedance matching* is the impedance matching between a transducer and the medium, such as water. A drawback with a single matching layer is that it only works effectively over a narrow frequency range, while the

actual acoustic pulse contains a fairly broad spectrum of frequencies. A better matching is achieved by using more than one matching layer, and it has been shown that a matching layer that has a continuously varying acoustic impedance across the layer provides broadband impedance matching.

Attenuation: Its Origin, Measurement, and Applications

Attenuation refers to the damping of a signal, here specifically an acoustic signal, with travel time or with travel distance. Attenuation is typically expressed in dB, i.e., on a logarithmic scale. Attenuation is an important parameter to measure in many types of materials characterization, but also the parameter that sets an upper limit for the ultrasound frequency that can be used for a given measurement. In NDE, attenuation is used for grain size estimation [8, 9], for characterization of composite materials, and for determination of porosity [10]. In medical ultrasound, attenuation can be used for tissue characterization [11], such as differentiating between normal and cirrhotic liver tissue and for classification of malignancies. In flowmeters, attenuation caused by vortices can be used to measure the frequency at which they are shed; this frequency is proportional to the flow velocity.

Attenuation represents the combined effect of *absorption* and *scattering*, where absorption refers to the conversion of acoustic energy into heat due to the viscosity of the medium, and scattering refers to the spreading of acoustic energy into other directions due to inhomogeneities in the medium. The absorption can, in part, be due to *classical absorption*, which varies with frequency squared, and *relaxation absorption*, which can result in a complicated frequency dependence of absorption. Gases (except for noble gases), liquids, and biological tissue exhibit mainly relaxation absorption, whereas classical absorption is most prominent in solids, which can also have a significant amount of scattering attenuation.

In general, absorption dominates in homogeneous media (e.g., liquids, gases, fine-grained metals, polymers), whereas scattering dominates in heterogeneous media (e.g., composites, porous ceramics, large-grained materials, bone). The actual attenuation and its frequency dependence can be specified fairly unambiguously for gases and liquids, while for solids it is very dependent on the manufacturing process, which determines the microstructure of the material, such as the grain structure.

Measurement of attenuation can be carried out for at least two purposes: (1) to measure the *bulk attenuation* of a given homogeneous medium; and (2) to measure the *spatial distribution of attenuation* over a plane in an inhomogeneous medium. The former approach is most common in materials characterization, whereas the latter approach is found mainly in medical ultrasound. Bulk attenuation can be performed either with transmission measurements or with pulse-echo measurements, as illustrated in Figure 26.36(a) and (b), respectively.

For the measurement of attenuation, in dB/cm, of a medium of thickness d , by transmission measurements, define $v_1(t)$ as the received signal without medium present and $v_2(t)$ as the received signal with medium present, as shown in Figure 26.36(a). The attenuation is then determined from the ratio of the energies of the two signals, corrected for the transmission losses, as:

$$\text{Att [dB/cm]} = \frac{1}{d} 10 \log \left\{ \frac{\int_0^{\infty} [v_1(t)]^2 dt}{\int_0^{\infty} [v_2(t)]^2 dt} \right\} - 20 \log \left\{ \frac{4z_1 z_2}{(z_1 + z_2)^2} \right\} \quad (26.34)$$

Correction for transmission losses (2nd term) can be avoided by alternatively measuring the incremental attenuation due to an incremental thickness increase.

For the measurement of attenuation by *pulse-echo measurements*, the front and the back wall echoes are termed $v_f(t)$ and $v_b(t)$, respectively. Based on an *a priori* knowledge of the pulse duration, a time window ΔT is defined. The attenuation is most accurately measured when based on the energies of $v_f(t)$ and $v_b(t)$, but may alternatively be based on the amplitudes of $v_f(t)$ and $v_b(t)$, as stated in Equation 26.35.

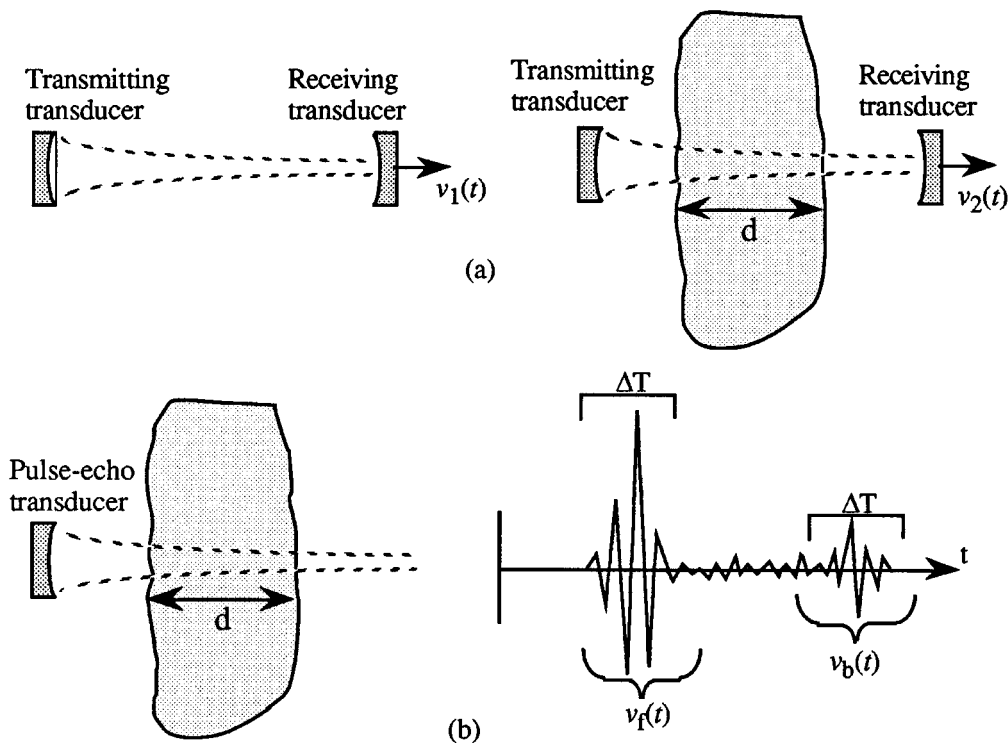


FIGURE 26.36 Measurement of bulk attenuation. (a) Measurement of attenuation by transmission measurement. (b) Measurement of attenuation by pulse-echo measurements.

$$\text{Att [dB/cm]} = \frac{1}{2d} 10 \log \left\{ \frac{\int_0^{\Delta t} [v_f(t)]^2 dt}{\int_0^{\Delta T} [v_b(t)]^2 dt} \right\} \cong \frac{1}{2d} 20 \log \left\{ \frac{\text{peak ampl., } v_f(t)}{\text{peak ampl., } v_b(t)} \right\} \quad (26.35)$$

Accurate attenuation measurements require attention to several potential pitfalls: (1) diffraction effects (even in the absence of attenuation, echoes from different ranges vary in amplitude, due to beam spreading); (2) misalignment effects (if the reflecting surface is not normal to the transducer axis, there is a reduction in detected signal amplitude, due to phase cancellation at the transducer surface); and (3) transmission losses whose magnitude it is not always easy to determine.

The spatial distribution of attenuation must be measured with pulse-echo measurements, where it is assumed that a backscatter signal of sufficient amplitude can be received from all regions of the medium. Use is made of the frequency dependence of attenuation, which has the effect that the shift in mean frequency of a given received echo relative to the mean frequency of the transmitted signal varies proportional to the total absorption. The *rate of shift* in mean frequency is thus proportional to the local attenuation.

CW Fields from Planar Piston Sources

In discussing the acoustic fields generated by acoustic radiators (transducers), a clear distinction must be made between fields due to CW excitation and due to pulse excitation. Although the overall field

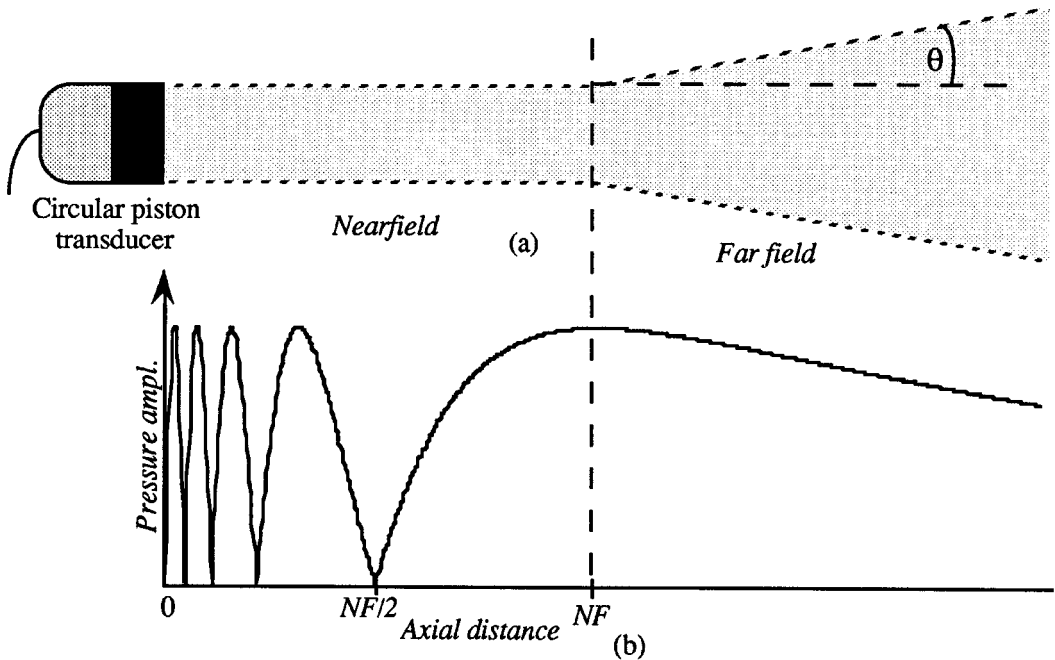


FIGURE 26.37 Pressure fields from a circular planar piston transducer operating with CW excitation. NF = Near Field. (a) Approximate field distribution in near field and far field. (b) Axial pressure in near field and far field for $(ka) = 31.4$.

patterns for these two cases are quite similar, the detailed field structure is very different. In this section, only CW fields are discussed.

When a CW excitation voltage is applied to a planar piston transducer, the resulting acoustic field can be divided into a *near field* region and a *far field* region. This division is particularly distinct when the transducer has a circular geometry. A piston transducer simply refers to a transducer with the same velocity amplitude at all points on the surface. The length of the near field, NF, is given as:

$$NF = \frac{a^2}{\lambda} \quad (26.36)$$

where a is the radius of the transducer and λ is the wavelength. As shown in [Figure 26.37\(a\)](#), the near field is approximately confined while the far field is diverging. The angle of divergence, θ , is approximately:

$$\theta = \arcsin\left(0.61 \frac{\lambda}{a}\right) \quad (26.37)$$

Additional comments to the simplified representation in [Figure 26.37\(a\)](#) are in order:

1. The actual field has no sharp boundaries, in contrast to what is shown in [Figure 26.37](#).
2. While the beam diameter is roughly constant in the near field, it is not as regular as shown; and at the same time, the near field structure is very complex.
3. The angle of divergence, θ , is only clearly established well into the far field.
4. The depiction of the far field shows only the main lobe; in addition, there are side lobes, which are directions of significant pressure amplitude, separated by *nulls* (i.e., directions with zero pressure amplitude).

In general, analytical expressions do not exist for the pressure magnitude at an arbitrary field point in the near field, and the pressure must instead be calculated by numerical techniques. However, an exact expression exists for the axial pressure amplitude, P_{ax} , valid in both near and far field [12].

$$P_{ax}(x) = 2 \rho_0 c_0 U_0 \left| \sin \left(0.5ka \left[\sqrt{x^2/a^2 + 1} - (x/a) \right] \right) \right| \quad (26.38)$$

In Equation 26.38, U_0 is the amplitude of the velocity function on the surface of the transducer. The expression is derived for a baffled planar piston transducer where the term “baffled” means that the transducer is mounted in a large rigid surface, called a baffle. Figure 26.37(b) shows the amplitude of the axial field for a planar piston transducer for which $(ka) = 31.4$. For field points located more than 3 to 4 near-field distances away from the transducer, a general expression for the pressure amplitude can be derived [12]:

$$P(r, \theta) = \frac{\rho_0 c_0}{2} U_0 ka \left(\frac{a}{r} \right) \left| \left[\frac{2J_1(ka \sin \theta)}{ka \sin \theta} \right] \right| \quad (26.39)$$

where $J_1(\cdot)$ is the Bessel function of the first order. The variable r is the length of the position vector defining the field point, and angle θ is the angle that the position vector makes with the x -axis.

Of interest in evaluating transducers in the far field is the *directivity*, D , defined as follows:

$$D(x) = \frac{I_{ax}(x) \left[\text{given source} \right]}{I_{ax}(x) \left[\text{simple source} \right]} \quad (26.40)$$

Thus, the directivity gives the factor with which the axial intensity of the given source is increased over that of a simple source (omnidirectional radiator), radiating the same total energy. For a baffled, circular planar piston transducer, the directivity in the far field can be calculated to be [12]:

$$D = \frac{(ka)^3}{ka - J_1(2ka)} \quad (26.41)$$

When $(2ka) \gg 1$, Equation 26.41 can be approximated to $D = (ka)^2$. Directivity values in the 1000s are common. For example, a 3.5 MHz transducer with 1 cm diameter radiating into water has a (ka) value of 73.3 and a directivity of 5373.

Often, focused transducers are used where the focusing is either created by the curvature of the piezoelectric element or by an acoustic lens in front of the transducer. The degree of focusing is determined by the (ka) value of the transducer.

Generation of Ultrasound: Piezoelectric and Magnetostrictive Phenomena

Ultrasound transducers today are available over a wide frequency range, in many sizes and shapes, and for a wide variety of applications. The behavior of the ultrasound transducer is determined by several parameters: the transduction material, the backing material, the matching layer(s), and the geometry and dimension of the transducer. A good overview of ultrasound transducers is available in [13].

The transduction material is most commonly a piezoelectric material, but can for some applications be a magnetostrictive material instead. These materials are inherently narrowband, meaning that they work efficiently only over a narrow frequency range. This is advantageous for CW applications such as

TABLE 26.3 List of Most Significant Piezoelectric Parameters for Common Piezoelectric Materials

Parameter	Barium titanate (BaTiO ₃)	Lead zirconate titanate, PZT-5	Lead meta-niobate, PbNb ₂ O ₆	Polyvinylidene fluoride (PVDF)
d_{33}	149 (10 ⁻¹² m/V)	374 (10 ⁻¹² m/V)	75 (10 ⁻¹² m/V)	22 (10 ⁻¹² m/V)
g_{33}	14 (10 ⁻³ Vm/N)	25 (10 ⁻³ Vm/N)	35 (10 ⁻³ Vm/N)	339 (10 ⁻³ Vm/N)
k_{33}	0.50	0.70	0.38	$k_{31} = 0.12$
k_T	0.38	0.68	0.40	0.11
Q_m	600	75	5	19

ultrasound welding and ultrasound hyperthermia, but is a problem for imaging applications, as impulse excitation will produce a long pulse with poor resolving abilities. To overcome this deficiency, a *backing material* is tightly coupled to the back side of the transducer for the purpose of damping the transducer and shortening the pulse. However, the backing material also reduces the sensitivity of the transducer. Some of this reduced sensitivity can be regained by the use of a *matching layer*, specifically selected for the medium of interest. As seen in Equation 26.33, a quarter wavelength matching layer can provide 100% efficient coupling to a medium, albeit only at one frequency. A combination of several matching layers can provide a more broadband impedance matching. The field is determined by both the geometry (planar, focused, etc.) of the transducer and by the frequency content of the velocity function of the surface of the transducer. In this section, unique aspects of the transduction material itself are described.

Piezoelectric Materials.

A piezoelectric material exhibits a mechanical strain (relative deformation) due to the presence of an electric field, and generates an electric field when subjected to a mechanical stress. A detailed review of piezoelectricity is given in [14]. Piezoelectric materials can either be: (1) natural material such as quartz; (2) man-made ceramics (e.g., barium titanate (BaTi), lead zirconate titanate (PZT), or lead meta-niobate); (3) man-made polymers (e.g., polyvinylidene fluoride (PVDF)). The piezoelectric ceramics are the most commonly used materials for ultrasound transducers. These ceramics are made piezoelectric by a so-called poling process in which the material is subjected to a strong electric field while at the same heating it to above the material's Curie temperature.

Several material constants determine the behavior of a given piezoelectric material, the most important of which are listed in Table 26.3 and defined below. An extensive list of parameter values for various piezoelectric materials is available in [15].

- d_{33} Transmission constant
- g_{33} Receiving constant
- k_{33} Piezoelectric coupling coefficient
- k_T Piezoelectric coupling coefficient for a transverse clamped material
- Q_M Mechanical Q

The transmission constant, d_{33} , gives the mechanical deformation of piezoelectric materials for frequencies well below the resonance frequency. A transducer with a large d_{33} value will therefore become an efficient transmitter. If an electric field, E_3 , is applied in the polarized direction of a piezoelectric rod or disk, the strain, S_3 , in that direction is approximately:

$$S_3 = d_{33} E_3 = d_{33} \frac{V_{\text{appl}}}{l} \quad (26.42)$$

where V_{appl} is the applied voltage and l is the thickness. The total deformation, Δl , becomes

$$\Delta l = d_{33} V_{\text{appl}} \quad (26.43)$$

The receiving constant, g_{33} , defines the sensitivity of a transducer element as a receiver when the frequency of the applied pressure is well below the resonance frequency of the transducer. If the applied stress (force/area) in the direction of polarization is T_3 , the output voltage from a rod or disk is approximately:

$$v_{\text{out}} = g_{33} T_3 l \quad (26.44)$$

The coupling coefficient describes the power conversion efficiency of a piezoelectric transducer, *operating at or near resonance*. Specifically, k_{33} is the coupling coefficient for an unclamped rod; that is, the rod is allowed to deform in the directions orthogonal to the direction of applied force or voltage. In contrast, k_T is the coupling coefficient for a *clamped* disk. Finally, Q_M gives the mechanical Q , which is a measure for how narrowband the transducer material inherently is.

Whereas expressions of the type given in Equations 26.42 to 26.44 are adequate for describing static or low-frequency behavior, the behavior near resonance where most transducers operate requires more complex models, which are beyond the scope of this chapter. The Mason model is adequate for narrowband modeling of transducers, whereas the KLM or Redwood models better describe the transducers for broadband applications [13, 15].

Magnetostrictive Materials.

The magnetostrictive phenomenon refers to a magnetically induced contraction or expansion in ferroelectric media, such as in nickel or alfenol, and was discovered by Joule in 1847. Magnetostrictive materials are generally used for ultrasound frequencies below 100 kHz, and are therefore relevant mainly for underwater applications. Eddy current losses influence the performance of magnetostrictive materials, but the losses can be reduced by constructing the magnetostrictive transducer from thin laminations.

Transducer Specifications.

Ultrasound transducers are generally specified by their diameter, center frequency, focal distance, and type of focusing (if applicable). The transducer can be designed as a contact transducer, a submersible transducer, an air transducer, etc.; in addition, the type of connector or cabling can be specified. In many cases, measurement data for the actual transducer can be supplied by the vendor in the form of a measured pressure pulse and the corresponding frequency spectrum, recorded with a hydrophone at a specific field point. Similarly, the beam profile can be measured in the form of pulse amplitude or pulse energy as a function of lateral position.

Detailed information about the acoustic field from a radiating transducer can be obtained with either the Schlieren technique or the optical interferometric technique. Such instruments are quite expensive, falling in the \$50K to \$120K range.

Display Formats for Pulse-Echo Measurements

The basic description of ultrasound imaging was presented earlier in this chapter. Based on the information presented so far in this section, more specific aspects of pulse-echo ultrasound imaging will now be described. Different display formats are used; the simplest of these is the *A-mode* display.

A-mode.

When a pulse-echo transducer has emitted a pulse in a given direction and has been switched to receive mode, an output signal from the transducer is produced based on detected echoes from different ranges, as illustrated conceptually in Figure 26.31(a). In this signal, distance to the reflecting structure has been converted into time from the start of signal. This signal is often referred to as the RF signal. Demodulating this signal (i.e., generating the envelope of the signal) produces the A-mode (amplitude mode) display, or the A-line signal. This signal can be the basis for range measurements, attenuation measurements, and measurement of reflection coefficient.

M-mode.

If the A-mode signal from a transducer in a fixed position is used to *intensity* modulate a cathode-ray tube (CRT), such as a monitor or oscilloscope, along a straight vertical line, a line of dots with brightness

according to echo strengths would appear on the screen. Moving the display electronically across the screen results in a set of straight horizontal lines. Now consider the case where the reflecting structures are moving in a direction toward or away from the transducer while pulse-echo measurements were being performed. This results in variations in the arrival time of echoes in the A-line signal, and the resulting lines across the screen are no longer straight, but curved, as determined by their velocity. Such a display is called *M-mode*, or motion mode, display. An application for this would be measurement of the diameter variation of a flexible tube, or blood vessel, due to a varying pressure inside the tube.

B-mode.

If pulse-echo measurements are repeatedly being performed, while the transducer scans the object of interest, an image of the object can be generated, as illustrated in Figure 26.31. Specifically, each A-line signal is used to intensity modulate a line on a CRT corresponding to the location of ultrasound beam, which produces an image that maps the reflectivity of the structures in the object. The resulting image is called a *B-mode* (or brightness mode) image. If the transducer is moved linearly, a rectangular image is produced, whereas a rotated transducer generates a pie-shaped, or sector image. This motion is typically done electronically or electromechanically, as described earlier under single-element and array transducers. When the scanning is done rapidly (say, 30 scans/s), the result is a real-time image.

Many forms of signal processing and image enhancement can be applied in the process of generating the B-mode image. Echoes from deeper lying structures will generally be of smaller amplitude, due to the attenuation of the overlying layers of the medium. Attenuation correction is made especially in medical imaging, so that echoes are displayed approximately with their true strength. This correction consists of a time-varying gain, called *time-gain control*, or TGC, such that the early arriving echoes experience only a low gain and later echoes from deeper lying structures experience a much higher gain. Various forms for signal compressions or nonlinear signal transfer function can selectively enhance the weaker or the stronger echoes.

C-mode.

In a C-mode display, only echoes from a specific depth will be imaged. To generate a complete image, the transducer must therefore be moved in a raster scan fashion over a plane. C-scan imaging is slow and cannot be used for real-time imaging, but has several applications in NDE for examining a given layer, or interface, in a composite structure, or the inner surface of a pipe.

Flow Measurements by Doppler Signal Processing

Flow velocity can be obtained by various ultrasonic methods (Chapter 28, Section 7), e.g., by measuring the Doppler frequency or Doppler spectrum. The Doppler frequency is the difference between the frequency (or pitch) of a moving sound source, as measured by a *stationary* observer, and the actual frequency of the sound source. The change in frequency is determined by the speed and direction of the moving source. The classical example is a moving locomotive with its whistle blowing; the pitch is increased when the train moves toward the observer, and vice versa. With respect to ultrasound measurements, only the reflecting (or scattering) gas, fluid, or structure is moving and not the the sound source, yet the Doppler phenomenon is present here as well. In order for ultrasound Doppler to function, the gas or fluid must contain scatterers that can reflect some of the ultrasound energy back to the receiver. The Doppler frequency, f_d , is given as follows:

$$f_d = \frac{2v}{c_0} \cos \theta \quad (26.45)$$

where v is the velocity of the moving scatterers, and θ is the angle between the velocity vector and the direction of the ultrasound beam. Doppler flowmeters require only access to the moving gas, fluid, or object from one side. For industrial use, when the fluids or gases often do not contain scatterers, *transmission* methods are preferred; these methods, however, are not based on the Doppler principle (Chapter 28, Section 7).

Two main categories of Doppler systems exist: the CW Doppler system and the PW (pulsed wave) Doppler system. The CW Doppler system transmits a continuous signal and does not detect the distance to the moving structure. It is therefore only applicable when there is just one moving structure or cluster of scatterers in the acoustic field. For example, a CW Doppler is appropriate for assessing the pulsatility and nature of blood flow in an arm or leg. CW Doppler systems are small and relatively inexpensive.

The PW Doppler system transmits a short burst at precise time intervals; it is therefore inherently a sampled system, and, as such, is subject to aliasing. It measures changes from one transmitted pulse to the next in the received signal from moving structures at one or several selected ranges, and is able to determine both velocity and range. Assuming that the ultrasound beam is narrow and thus very directional, the PW Doppler can create a *flow image*; that is, it can indicate the magnitude and direction of flow over an image plane. Commonly, color and color saturation are used to indicate direction and speed in a flow image, respectively. In contrast to CW Doppler systems, the PW Doppler systems require much signal processing and are therefore typically expensive and often part of a complete imaging system. When a distribution of velocities, rather than a single velocity, is encountered, as is often the case with fluid flow, a Doppler spectrum rather than a Doppler frequency is determined. An FFT (Fast Fourier Transform) routine is then used to reveal the Doppler frequencies and thus the velocity components present.

Review of Common Applications of Ultrasound and Their Instrumentation

Range Measurements, Air

Ultrasound range measurements are used in cameras, in robotics, for determining dimensions of rooms, etc. Measurement frequencies are typically around 50 kHz to 60 kHz. The measurement concept is pulse-echo, but with burst excitation rather than pulse excitation. Special electronic circuitry and a thin low-acoustic-impedance air transducer is most commonly used. Rugged solid or composite piezoelectric-based transducers, however, can also be used, sometimes up to about 500 kHz.

Thickness Measurement for Testing, Process Control, Etc.

Measurement of thickness is a widely used application of ultrasound. The measurements can be done with direct coupling between the transducer and the object of interest, or — if good surface contact is difficult to establish — with a liquid or another coupling agent between the transducer and the object. Ultrasound measurements of thickness have applications in process control, quality control, measuring build-up of ice on an aircraft wing, detecting wall thickness in pipes, as well as medical applications. The instrumentation involves a broadband transducer, pulser-receiver, and display or, alternatively, echo detecting circuitry and numerical display.

Detection of Defects, such as Flaws, Voids, and Debonds

The main ultrasound application in NDE is inspection for the localization of voids, crack, flaws, debonding, etc. [3]. Such defects can exist immediately after manufacturing, or were formed due to stresses, corrosion, etc. Various types of standard or specialized flaw detection equipment are available from ultrasound NDE vendors.

Doppler Flow Measurements

The flow velocity of a liquid or a moving surface can be determined through Doppler measurements, provided that the liquid or the surface scatters ultrasound back in the direction of the transducer, and that the angle between the flow direction and the ultrasound beam is known. Further details are given in the section about Doppler processing. CW and PW Doppler instruments are commercially available, with CW instrumentation being by far the least expensive.

Upstream/Downstream Volume Flow Measurements

When flow velocity is measured in a pipe with access to one or both sides, an ultrasound transmission technique can be used in which transducers are placed on the same or opposite sides of the pipe, with

one transducer placed further upstream than the other transducer. From the measured *difference* in travel time between the upstream direction and the downstream direction, and knowledge about the pipe geometry, the volume flow can be determined. Special clamp-on transducers and instrumentation are available. An overview of flow applications in NDE is given in [16].

Elastic Properties of Solids

Since bulk sound speed varies with the elastic stiffness of the object, as given in Equation 26.15, sound speed measurements can be used to estimate elastic properties of solids under different load conditions and during solidification processes. Such measurements can also be used for measurement of product uniformity and for quality assurance. The measurements can be performed on bulk specimens or on thin rods, using either pulse-echo or transmission instrumentation [17]. Alternatively, measurements of the material's own resonance frequencies can be performed for which commercial instruments, such as the *Grindo-sonics*, are available.

Porosity, Grain Size Estimation

Measurement of ultrasound attenuation can reveal several materials parameters. By observing the attenuation in metals as a function of frequency, the grain size and grain size distribution can be estimated. Attenuation has been used for estimating porosity in composites. In medical ultrasound, attenuation is widely used for tissue characterization, that is, for differentiating between normal and pathological tissues. Pulse-echo instrumentation interfaced with a digitizer and a computer for data analysis is required.

Acoustic Microscopy

The measurement approaches utilized in acoustic microscopy are similar to other ultrasound techniques, in that A-scan, B-scan, and C-scan formats are used. It is in the applications and the frequency ranges where acoustic microscopy differs from conventional pulse-echo techniques. Although acoustic microscopes have been made with transducer frequencies up to 1 GHz, the typical frequency range is 20 MHz to 100 MHz, giving spatial resolutions in the range from 100 μm to 25 μm . Acoustic microscopy is used for component failure analysis, electronic component packaging, and internal delaminations and dis-bonds in materials, and several types of acoustic microscopes are commercially available.

Medical Ultrasound

Medical imaging is a large and diverse application area of ultrasound, especially in obstetrics, cardiology, vascular studies, and for detecting lesions and abnormalities in organs. The display format is either B-mode, using gray scale image, or a combination of Doppler and B-mode, with flow presented in color and stationary structures in gray scale. A wide variety of instruments and scanners for medical ultrasound are available.

Selected Manufacturers of Ultrasound Products

Table 26.4 contains a representative list of ultrasound equipment and manufacturers.

Advanced Topics in Ultrasound

Overview of Diffraction

The ultrasound theory presented thus far has emphasized basic concepts, and the applications that have been discussed tacitly assume that the field from the transducer is a plane wave field. This simplifying assumption is acceptable for applications such as basic imaging and measurements based on travel time. However, the plane wave assumption introduces errors when materials parameters (e.g., attenuation, surface roughness, and object shape) are sought to be measured with ultrasound. Therefore, to use ultrasound as a quantitative tool, an understanding is needed of the structure of the radiated acoustic field from a given transducer with a given excitation, and — equally important — the ability to calculate the actual radiated field. This leads to the topic of diffraction, which is the effect that accounts for the complex structure of both radiated and scattered fields. Not surprisingly, there are direct parallels between optical diffraction and acoustic diffraction. (As a separate issue, it should be noted that the ultrasound

TABLE 26.4 List of Products for and Manufacturers of Ultrasound Measurements

Product type	Manufacturer
Ultrasound transducers	Panametrics, 221 Crescent St., Waltham, MA 02154. (800) 225-8330
Ultrasound transducers	Krautkramer Branson Inc., 50 Industrial Park Rd., Lewistown, PA 17044. (717) 242-0327
Range measurements, air	Polaroid Corporation, Ultrasonics Components Group, 119 Windsor Street, Cambridge, MA 02139. (800) 225-1618
Pulser-receivers	Panametrics, 221 Crescent St., Waltham, MA 02154. (800) 225-8330
Pulser-receivers	JSR Ultrasonics, 3800 Monroe Ave., Pittsfield, NY 14534. (716) 264-0480
Ultrasound power ampl.	Amplifier Research, 160 School House Rd., Souderton, PA 18964. (800) 254-2677
Ultrasound power ampl.	Ritec, 60 Alhambra Rd., Suite 5, Warwick, RI 02886. (401) 738-3660
NDE instrumentation	Panametrics, 221 Crescent St., Waltham, MA 02154. (800) 225-8330
NDE instrumentation	Krautkramer Branson Inc., 50 Industrial Park Rd., Lewistown, PA 17044. (717) 242-0327
Acoustic microscopy	Sonoscan, 530 E. Green St., Bensenville, IL 60106. (708) 766-4603
Medical Imaging	Hewlett Packard, Andover, MA; ATL, Bothell, WA; Diasonics, Milpitas, CA; Siemens Ultrasound, Issaquah, WA.
Schlieren based imaging of acoustic fields	Optison, 568 Weddell Drive, Suite 6, Sunnyvale, CA 94089. (408) 745-0383
Optical based imaging of acoustic fields	UltraOptec, 27 de Lauzon, Boucherville, Quebec, Canada J4B 1E7. (514) 449-2096

theory presented here assumes that the wave amplitudes [pressure, displacement] are small enough so that nonlinear effects can be disregarded.)

Diffraction is basically an edge effect. Whereas a plane wave incident on a large planar interface is reflected in a specific direction, the plane wave incident on an edge results in waves scattered in many directions. Similar considerations hold for the field produced by a transducer: The surface of the transducer produces a so-called *geometric wave* that has the shape of the transducer itself; the edge of the transducer, however, generates an *edge wave* with the shape of an expanding torus. The actual pressure field is a combination of the two wave fields. Very close to a large transducer, the geometric wave dominates, and diffraction effects might not need to be considered. Over small regions far away from the transducer, the field can be approximated by a plane wave field, and diffraction does not need to be considered. However, in many practical cases, diffraction must be considered if detailed information about the pressure field is desired, and numerical methods must be employed for the calculations.

The structure of the axial field, shown in Figure 26.37(b), is a direct result of diffraction. Numerical evaluation of the diffracted field from a transducer can be done in several ways: (1) use of the Fresnel or Fraunhofer integrals (not applicable close to the transducer) to calculate the field at a single frequency at a specified plane normal to the transducer axis; (2) calculation of the pressure function at any point of interest in space, based on a specified velocity function, $u(t)$, on the surface of the transducer, using Rayleigh integral; (3) decomposing the velocity field in the plane of the transducer into its plane wave components, using a 2-D Fourier transform technique, followed by a forward propagation of the plane waves to the plane of interest and an inverse Fourier transform to give the diffracted field; or (4) use of finite element methods to calculate the diffracted field at any point or plane of interest. In the following, methods (1) and (2) will be described.

Fresnel and Fraunhofer Diffraction.

Let the velocity function on the surface of the transducer, $u(x, y)$, be specified for a particular frequency, ω . Assume that the transducer is located in the $(x, y, 0)$ plane and that one is interested in the pressure field in the (x_0, y_0, z) plane. The Fresnel diffraction formulation [18] assumes that the paraxial approximation is fulfilled, requiring z to be at least 5 times greater than the transducer radius, in which case the *Fresnel diffraction integral* applies:

$$p(x_0, y_0, z, \omega) = \frac{A_0}{\lambda_z} \iint_S u(x, y, \omega) \exp\left[-jk \frac{x^2 + y^2}{2z}\right] \exp\left[jk \frac{x_0 x + y_0 y}{z}\right] dx dy \quad (26.46)$$

where S is the surface of the transducer and A_0 is a constant. If one defines the two first terms of the integrand as some complex spatial function, $\Gamma(x,y)$, then Equation 26.46 is a scaled Fourier transform of $\Gamma(x,y)$.

If $k(x^2 + y^2)/2z \ll 1$, or, equivalently, $z > 10 a^2/\lambda$, the second term in Equation 26.46 can be ignored, and the resulting equation is called the *Fraunhofer diffraction integral*:

$$p(x_0, y_0, z, \omega) = \frac{A_0}{\lambda z} \iint_S u(x, y, \omega) \exp\left[jk \frac{x_0 x + y_0 y}{z}\right] dx dy \quad (26.47)$$

Thus, one can only use the Fraunhofer integral for calculating the far field diffraction. From Equation 26.47, one can make the interesting observation that the far field of a transducer is a scaled version of the Fourier transform of the source.

Pressure Function at a Given Field Point, Based on Rayleigh Integral.

While the Fresnel and Fraunhofer diffraction methods are CW methods, calculation of pressure from the Rayleigh integral is fundamentally an impulse technique, and is as such better suited for analysis of pulse-echo measurements. The basis for the calculation is the *velocity potential impulse response*, $h(\vec{r}, t)$, obtained from the Rayleigh integral:

$$h(\vec{r}, t) = \frac{1}{2\pi} \iint_S \frac{\delta(t - r'/c)}{r'} dS \quad (26.48)$$

In Equation 26.48, r' is the distance from dS on the surface of the transducer to the field point, defined by the position vector \vec{r} , and $\delta(t)$ is the Dirac delta function. As can be seen, $h(\vec{r}, t)$ is the result of an impulsive velocity excitation on the surface of the transducer and is a function of both time and a spatial location. It is important to note that $h(\vec{r}, t)$ exists in analytical form for several transducer geometries, and, by extension, for annular and linear array transducers [19].

For the case of an arbitrary velocity function, $u(t)$, on the transducer surface, the corresponding velocity potential, $\phi(\vec{r}, t)$, is obtained as:

$$\phi(\vec{r}, t) = u(t) \otimes h(\vec{r}, t) \quad (26.49)$$

where \otimes refers to time domain convolution. Both particle velocity, $u(\vec{r}, t)$, and pressure, $p(\vec{r}, t)$, can be found from $\phi(\vec{r}, t)$, as follows:

$$u(\vec{r}, t) = \nabla \phi(\vec{r}, t) \quad (26.50)$$

$$p(\vec{r}, t) = -\rho_0 \frac{\partial}{\partial t} \phi(\vec{r}, t) \quad (26.51)$$

where ∇ is the gradient operator.

Thus, from the expressions above, the pressure can be calculated for any field point, \vec{r} , when $u(t)$ and the transducer geometry are defined. In this calculation, all diffraction effects are included. However, given the high frequency content in $h(\vec{r}, t)$ and in particular in the time derivative of $h(\vec{r}, t)$, care must be taken to avoid aliasing errors, as described in [19].

Received Signal in Pulse-Echo Ultrasound.

The expression in Equation 26.51 allows for quantitative evaluation of the pressure field for an arbitrary point, line, or plane. However, it does not describe the calculation of the received signal in a pulse-echo

system. Consider a small planar reflector, placed in a homogeneous medium, and referred to as dR . The reflector has the area dA . The dimensions of dR must be small with respect to the shortest wavelength in the insonifying pulse. The location and the orientation of the planar reflector is given by \vec{r} and \vec{n} , respectively, where \hat{n} is a unit normal vector to the small reflector.

The voltage from the receiving transducer in a pulse-echo system due to dR is termed $d v(\vec{r}, t)$ and can be determined when $u(t)$ is specified. The electro-acoustic transfer function for both the transmitting and the receiving transducer is assumed to be unity for all frequencies. For the case when the acoustic impedance of dR is much higher than that of the medium, $d v(\vec{r}, t)$ is given as [20]:

$$\begin{aligned} d v(\vec{r}, t) &= A_0 \rho_0 \frac{\cos[\psi(\vec{r})]}{c_0} \left[h(\vec{r}, t) \otimes h(\vec{r}, t) \otimes \frac{\partial^2}{\partial t^2} u(t) \right] dA \\ &= A_0 \cos[\psi(\vec{r})] u(t) \otimes \frac{\rho_0}{c_0} \left[\frac{\partial^2}{\partial t^2} (h(\vec{r}, t) \otimes h(\vec{r}, t)) \right] dA \end{aligned} \quad (26.52)$$

In Equation 26.52, A_0 is determined by the reflection coefficient of the reflector. The term $\cos[\psi(\vec{r})]$ is a correction term (obliquity factor) where $\psi(\vec{r})$ is the angle between \hat{n} and the propagation direction of the wave field at \vec{r} . For an extended surface, the received voltage can be found by decomposing the surface into small reflectors and calculating the total received signal as the sum of the contributions from all the small reflectors. An efficient numerical technique for this type of integration has been developed [21].

References

1. C. M. Fortunko and D. W. Fitting, Appropriate ultrasonic system components for NDE of thick polymer-composites, *Review of Progress in Quantitative Nondestructive Evaluation, Vol. 10B*. New York: Plenum Press, 1991, 2105-2112.
2. C. R. Hill, Medical imaging and pulse-echo imaging and measurement, in C.R. Hill (ed.) *Physical Principles of Medical Ultrasound*, New York: Halsted Press, 1986, chaps. 7 and 8, 262-304.
3. L. C. Lynnworth, *Ultrasonic Measurements for Process Control*, San Diego: Academic Press, 1989, 53-89.
4. L. E. Kinsler, A. R. Frey, A. B. Coppens, and J. V. Sanders, *Fundamentals of Acoustics*, 3rd. ed., New York: John Wiley, 1982, 106.
5. J. D. Achenbach, *Wave Propagation in Elastic Solids*, 1st ed., New York: Elsevier Science, 1975, 123.
6. L. E. Kinsler, A. R. Frey, A. B. Coppens, and J. V. Sanders, *Fundamentals of Acoustics*, 3rd. ed., New York: John Wiley, 1982, 115-117.
7. L. E. Kinsler, A. R. Frey, A. B. Coppens, and J. V. Sanders, *Fundamentals of Acoustics*, 3rd. ed., New York: John Wiley, 1982, 127-133.
8. J. Saniie and N. M. Bilgutay, Quantitative grain size evaluation using ultrasonic backscattered echoes, *J. Acoust. Soc. Am.*, 80, 1816-1824, 1986.
9. E. P. Papadakis, Scattering in polycrystalline media, in P. D. Edmonds (ed.) *Ultrasonics*, New York: Academic Press, 1981, 237-298.
10. S. M. Handley, M. S. Hughes, J. G. Miller, and E. I. Madaras, Characterization of porosity in graphite/epoxy laminates with polar backscatter and frequency dependent attenuation, *1987 Ultrasonics Symp.*, 1987, 827-830.
11. J. C. Bamber, Attenuation and absorption, in C.R. Hill (ed.), *Physical Principles of Medical Ultrasound*, New York: Halsted Press, 1986, 118-199.
12. L. E. Kinsler, A. R. Frey, A. B. Coppens, and J. V. Sanders, *Fundamentals of Acoustics*, 3rd. ed., New York: John Wiley, 1982, 176-185.
13. M. O'Donnell, L. J. Busse, and J. G. Miller, Piezoelectric transducers, in P. D. Edmonds (ed.), *Ultrasonics*, New York: Academic Press, 1981, 29-65.

14. IEEE Standard on Piezoelectricity, *IEEE Trans. Sonics Ultrasonics*, 31, 8–55, 1984.
15. G.S. Kino, *Acoustic Waves*, Englewood Cliffs, NJ: Prentice-Hall, 1987, 17-83 and 554-557.
16. L. C. Lynnworth, *Ultrasonic Measurements for Process Control*, San Diego, CA: Academic Press, 1989, 245-368.
17. L. C. Lynnworth, *Ultrasonic Measurements for Process Control*, San Diego, CA: Academic Press, 1989, 537-557.
18. V. M. Ristic, *Principles of Acoustic Devices*, New York: John Wiley & Sons, 1983, 316-320.
19. D. P. Orofino and P. C. Pedersen, Multirate digital signal processing algorithm to calculate complex acoustic pressure fields, *J. Acoust. Soc. Am.*, 92, 563-582, 1992.
20. A. Lhemery, Impulse-response method to predict echo responses from targets of complex geometry. I. Theory, *J. Acoust. Soc. Am.*, 90, 2799-2807, 1991.
21. S. K. Jespersen, P. C. Pedersen, and J. E. Wilhjelm, The diffraction response interpolation method, *IEEE Trans. Ultrasonics, Ferroelectrics, and Frequency Control*, 45, Nov. 1998.

Further Information

- L. C. Lynnworth, *Ultrasonic Measurements for Process Control*, San Diego, CA: Academic Press, 1989, an excellent overview of industrial applications of ultrasound.
- L. E. Kinsler, A. R. Frey, A. B. Coppens, and J. V. Sanders, *Fundamentals of Acoustics*, 3rd. ed., New York: John Wiley & Sons, 1982, a very readable introduction to acoustics.
- P. D. Edmonds (ed.), *Ultrasonics*, (Vol. 19 in the series: *Methods of Experimental Physics*). New York: Academic Press, 1981, in-depth description of ultrasound interaction with many types of materials, along with discussion of ultrasound measurement approaches.
- J. A. Jensen, *Estimation of Blood Velocities Using Ultrasound*, Cambridge, UK: Cambridge University Press, 1996, a very up-to-date book about ultrasound Doppler measurement of flow and the associated signal processing.
- E. P. Papadakis (ed.), *Ultrasonic Instruments and Devices: Reference for Modern Instrumentations, Techniques, and Technology*, in the series *Physical Acoustics*, Vol. 40, New York: Academic Press, 1998.
- F. W. Kremkau, *Diagnostic Ultrasound: Principles and Instruments*, 5th ed., Philadelphia, PA: W. B. Saunders Co., 1998, a very readable and up-to-date introduction to medical ultrasound.